Effect of Global Sea Level Rise over the Near, Intermediate and Long-Term on Tsunami Waves at the Victoria Coast Guard Station in Southwestern British Columbia

Richard Thomson, Alexander Rabinovich, Lauren Lupton, Stephen Mundschutz and Nicky Hastings

Fisheries and Oceans Canada
Institute of Ocean Sciences
9860 West Saanich Road
Sidney, BC V8L 4B2

2023

Canadian Technical Report of
Hydrography and Ocean Sciences 362

Fisheries and Oceans Canada | Pêches et Océans Canada

Canada

Canadian Technical Report of Hydrography and Ocean Sciences

Technical reports contain scientific and technical information of a type that represents a contribution to existing knowledge, but which is not normally found in the primary literature. The subject matter is generally related to programs and interests of the Oceans and Science sectors of Fisheries and Oceans Canada.

Technical reports may be cited as full publications. The correct citation appears above the abstract of each report. Each report is abstracted in the data base Aquatic Sciences and Fisheries Abstracts.

Technical reports are produced regionally but are numbered nationally. Requests for individual reports will be filled by the issuing establishment listed on the front cover and title page.

Regional and headquarters establishments of Ocean Science and Surveys ceased publication of their various report series as of December 1981. A complete listing of these publications and the last number issued under each title are published in the Canadian Journal of Fisheries and Aquatic Sciences, Volume 38: Index to Publications 1981. The current series began with Report Number 1 in January 1982.

Rapport technique canadien sur l'hydrographie et les sciences océaniques

Les rapports techniques contiennent des renseignements scientifiques et techniques qui constituent une contribution aux connaissances actuelles mais que l'on ne trouve pas normalement dans les revues scientifiques. Le sujet est généralement rattaché aux programmes et intérêts des secteurs des Océans et des Sciences de Pêches et Océans Canada.

Les rapports techniques peuvent être cités comme des publications à part entière. Le titre exact figure au-dessus du résumé de chaque rapport. Les rapports techniques sont résumés dans la base de données Résumés des sciences aquatiques et halieutiques.

Les rapports techniques sont produits à l'échelon régional, mais numérotés à l'échelon national. Les demandes de rapports seront satisfaites par l'établissement auteur dont le nom figure sur la couverture et la page de titre.

Les établissements de l’ancien secteur des Sciences et Levés océaniques dans les régions et à l'administration centrale ont cessé de publier leurs diverses séries de rapports en décembre 1981. Vous trouverez dans l'index des publications du volume 38 du Journal canadien des sciences halieutiques et aquatiques, la liste de ces publications ainsi que le dernier numéro paru dans chaque catégorie. La nouvelle série a commencé avec la publication du rapport numéro 1 en janvier 1982.

Canadian Technical Report of
Hydrography and Ocean Sciences 362

2023

EFFECT OF GLOBAL SEA LEVEL RISE OVER THE NEAR, INTERMEDIATE AND LONG-TERM ON TSUNAMI WAVES AT THE VICTORIA COAST GUARD STATION IN SOUTHWESTERN BRITISH COLUMBIA

Richard Thomson[1], Alexander Rabinovich[1], Lauren Lupton[1], Stephen Mundschutz[1], and Nicky Hastings[2]

[1]Fisheries and Oceans Canada
Institute of Ocean Sciences
9860 West Saanich Road
Sidney, BC V8L 4B2

[2]Natural Resources Canada
Geological Survey of Canada - Pacific Division
605 Robson Street
Vancouver, BC V6B 5J3

Cat. No. Fs97-18/362E-PDF ISBN 978-0-660-68321-8 ISSN 1488-5417

Correct citation for this publication:

Thomson, R., Rabinovich, A., Lupton, L., Mundschutz, S., and Hastings, N., 2023. Effect of global sea level rise over the near, intermediate and long-term on tsunami waves at the Victoria Coast Guard Station in southwestern British Columbia. Can. Tech. Rep. Hydrogr. Ocean Sci. 362: v + 61 p.

CONTENTS

ABSTRACT

Thomson, R., Rabinovich, A., Lupton, L., Mundschutz, S., and Hastings, N., 2023. Effect of global sea level rise over the near, intermediate and long-term on tsunami waves at the Victoria Coast Guard Station in southwestern British Columbia. Can. Tech. Rep. Hydrogr. Ocean Sci. 362: v + 61 p.

The coast of British Columbia is susceptible to flooding and strong currents from trans-oceanic tsunamis. Global sea level rise and vertical tectonic land motions further compound the effects of future tsunamigenic events. The present study centres on the Victoria Coast Guard Station in Victoria Harbour. We examine historical tsunamis observed at this site and the results of numerical modelling of the two potentially most dangerous Victoria region tsunamis – a 1964-type Alaska and a 1700-type Cascadia Subduction Zone (CSZ) tsunami – and estimate the risk for the region taking into account vertical tectonic motion and climatic sea level change.

Of the 39 tsunamis recorded at Victoria between 1910 and 2021, only the 1964 magnitude 9.2 event generated tsunami waves that were hazardous to the Victoria area (maximum wave amplitude, 70 cm). Centuries earlier, the magnitude 9.0 CSZ earthquake of 26 January 1700 generated a trans-oceanic tsunami that also strongly affected the British Columbia coast. Such an event is likely to occur again sometime in the next 500 to 700 years.

Based on reports by the United Nations Intergovernmental Panel on Climate Change (IPCC), James et al. [2015; 2021] and Lemmen et al. [2016] examined sea level rise in western Canada that takes into account both climatic effects and vertical tectonic motions for *low, moderate* and *high* global sea level rise scenarios. These findings enabled us to estimate the effect that sea-level changes will have on future tsunamis impacting the entire British Columbia coast. Detailed results focus on Victoria Harbour in the southwest corner of the province.

RÉSUMÉ

Thomson, R., Rabinovich, A., Lupton, L., Mundschutz, S., and Hastings, N., 2023. Effect of global sea level rise over the near, intermediate and long-term on tsunami waves at the Victoria Coast Guard Station in southwestern British Columbia. Can. Tech. Rep. Hydrogr. Ocean Sci. 362: v + 61 p.

La côte de la Colombie-Britannique est vulnérable aux inondations et aux forts courants provoqués par les tsunamis transocéaniques. L'élévation du niveau de la mer à l'échelle mondiale et les mouvements tectoniques verticaux des terres aggravent encore les effets des futurs événements tsunamigènes. La présente étude se concentre sur la station de la Garde côtière de Victoria, dans le port de Victoria. Nous examinons les tsunamis historiques observés sur ce site et les résultats de la modélisation numérique des deux tsunamis potentiellement les plus dangereux de la région de Victoria – un tsunami de type 1964 en Alaska et un tsunami de type 1700 dans la zone de subduction de Cascadia (CSZ) – et estimons le risque pour la région en prenant en compte le mouvement tectonique vertical et le changement climatique du niveau de la mer.

Sur les 39 tsunamis enregistrés à Victoria entre 1910 et 2021, seul celui de 1964, d'une magnitude de 9,2, a généré des vagues de tsunami dangereuses pour la région de Victoria (amplitude maximale des vagues, 70 cm). Des siècles plus tôt, le séisme de magnitude 9,0 CSZ du 26 janvier 1700 avait généré un tsunami transocéanique qui avait également fortement touché la côte de la Colombie-Britannique. Un tel événement est susceptible de se reproduire dans les 500 à 700 prochaines années.

Sur la base des rapports du Groupe d'experts intergouvernemental sur l'évolution du climat (GIEC) des Nations Unies, James et al. [2015 ; 2021] et Lemmen et al. [2016] ont examiné l'élévation du niveau de la mer dans l'ouest du Canada en tenant compte à la fois des effets climatiques et des mouvements tectoniques verticaux pour des scénarios d'élévation mondiale du niveau de la mer faibles, modérés et élevés. Ces résultats nous ont permis d'estimer l'effet qu'auront les changements du niveau de la mer sur les futurs tsunamis touchant l'ensemble de la côte de la Colombie-Britannique. Les résultats détaillés se concentrent sur le port de Victoria, dans le sud-ouest de la province.

1 INTRODUCTION

Large segments of the British Columbia coast are susceptible to tsunamis generated by major earthquakes within the Pacific Ocean and by local underwater earthquakes. The catastrophic tsunamis of the last two decades, including the 2004 Sumatra, 2010 Chile and 2011 Tohoku events, as well as two recent 2018 tsunamis in Indonesia (Sulawesi and Anak-Krakatau), demonstrate the serious threat of major seismically generated tsunamis to various regions of the world's oceans, including coastal communities in southern British Columbia, in particular Victoria [cf. *Clague et al.*, 2003; *Leonard et al.*, 2014]. The eastern part of Juan de Fuca Strait is partially sheltered from tsunami waves incoming from the open ocean; nevertheless, tsunamis from major events (e.g., the 1964 Alaska and 2011 Tohoku tsunamis) have penetrated into the region where they have been recorded by CHS and NOAA tide gauges. The 1964 Alaska ("Good Friday") earthquake (M_w 9.2) produced the strongest tsunami response ever observed on the coast of British Columbia and caused about $10 million in damage (1964-dollar values) [*Rabinovich et al.*, 2019].

A major tsunami generated in the Cascadia Subduction Zone (CSZ) deserves specific attention. The Great CSZ earthquake of 26 January 1700 with an estimated magnitude M_w 9.0 formed a major

trans-oceanic tsunami that caused significant destruction in Japan on the opposite side of the Pacific Ocean [cf. *Atwater et al.,* 2005], and strongly affected the outer coast of British Columbia. Paleotsunami findings in the coastal zone of Vancouver Island [cf. *Clague et al*., 2000, 2003] show that tsunami waves of ~15 m likely struck this coast at the time of the 1700 CSZ event.

Vertical tectonic motions and changing climate are crucial factors that contribute to significant regional and global sea level variations and, in this way, can substantially increase the risk of marine sea level hazards impacting the coastal regions of British Columbia. The global climatic effects include changes in air and water temperature, precipitation patterns, wave climate, sea ice, hydrology (including glacier melting) and ocean-water properties (e.g., salinity and density). These changes exacerbate existing risks and bring new challenges to coastal engineers and emergency response managers.

Several observational and numerical modelling studies have been conducted recently on various types of natural hazards in the Southern Strait of Georgia. *Fine et al.* [2018a, 2018b] numerically simulated the 1964 Great Alaska and the 1700 Cascadia Subduction Zone (CSZ) tsunamis, focussing on the southern part of Vancouver Island and specifically on the Victoria region. *Rabinovich et al*. [2019] collected all available observations, modelling results and other information to estimate the main statistical parameters of five major trans-oceanic tsunamis during the "recent" observational period (1946, 1952, 1957, 1960 and 1964) along the coast of British Columbia, including Victoria and other tide gauge stations located nearby.

In recent years, the United Nations Intergovernmental Panel on Climate Change (IPCC) published several reports, in particular the 2019 ICPC Special Report on the Ocean and Cryosphere in a Changing Climate (SROCC) with a specific Chapter 4 on sea level rise [*Oppenheimer and Glavovic*, 2019]. Also, *James et al.* [2015, 2021] and *Lemmen et al.* [2016] prepared special reports considering sea level rise in western Canada that takes into account both global climatic sea level rise and vertical tectonic motions on the coast of British Columbia. *Rabinovich and Thomson* [2020] evaluated vertical tectonic motions and changing sea levels along the southeastern coast of Vancouver Island for *low, moderate* and *high* global sea level rise scenarios; the corresponding findings were used to estimate expected coastal flooding due to major trans-oceanic tsunamis and other marine hazards for this coast focussing on the Canadian Coast Guard Station in Victoria.

The purpose of the present report is to summarize previous findings and to examine changes to the existing estimates of coastal flooding to the Canadian Coast Guard Station in Victoria due to

major trans-oceanic tsunamis and sea level rise. In Section 2, we estimate the tsunami risk for Victoria based on all available observational data for the period of 1910-2020. Section 3 examines the main modelling results of *Fine et al.* [2018a, 2018b] for the 1964 Alaska and the 1700 CSZ tsunamis for the Victoria area. In Section 4, we consider sea level rise for Victoria caused by the combined effect of climate change and vertical tectonic motions. The results of Sections 3 and 4 are merged in Section 5, while the general conclusions are given in Section 6.

2 HISTORICAL AND RECENT TSUNAMIS AT VICTORIA

Sea level measurements on the coast of British Columbia have been performed by the Canadian Hydrographic Service (CHS) for more than 110 years. The first tide gauge stations to operate on a permanent basis in British Columbia began in 1906-1909 at Victoria (Juan de Fuca Strait, the southeastern coast of Vancouver Island), Tofino (oceanic, southwestern coast of Vancouver Island), Prince Rupert (the head of Dixon Entrance, the northern mainland coast), Caulfeild/Point Atkinson (the Strait of Georgia, near West Vancouver) and Vancouver (within Burrard Inlet). These five stations have the longest records for the Pacific coast of Canada and, in general, among the longest records in North America. Prince Rupert, Tofino and Victoria have the longest records of tsunami events on the Pacific coast [*Rabinovich et al.*, 2019].

Between 1910 and 1997, all tide gauges on the B.C. coast were analogue ("pen-and-paper"). Tides are relatively high on the coast of British Columbia and in some locations exceed 6 m (Thomson, 1981). Such large tides made the detection of relatively weak tsunamis from paper records almost impossible. Moreover, the reliable direct estimation of tsunami parameters was problematic even for great tsunamis, especially for those that have long-period signals. The catastrophic tsunamis of the 1990s initiated (1997-1998) a major upgrade of the existing tsunami warning and Permanent Water Level Network (PWLN) stations on the B.C. coast. The new digital instruments were designed to continuously measure sea level variations with much higher precision than the earlier analogue gauges, and to store corresponding sea level samples every minute [*Rabinovich and Stephenson*, 2004]. These new instruments made it possible to detect even weak tsunamis and accurately estimate their parameters [*Stephenson and Rabinovich*, 2009].

Tofino is the "beacon station" for the west coast of Canada and one of the most important "tsunami warning stations" for the entire Pacific coast of North America [*Wigen*, 1983; *Rabinovich*

and Stephenson, 2004]. Almost all seismically generated tsunamis observed since 1910 along the coast of British Columbia, were instrumentally recorded at this station (Figure 1a). For this reason, we use Tofino as the *reference station* in our study of tsunamis at Victoria. During the entire 110-year observational period, there were no tsunami events (except local meteorological tsunamis) that were recorded at Victoria but not at Tofino.

During the period 1910-2020, a total of 70 tsunamis were detected at Tofino: 42 during the "analogue period" of 1910-1999 and 28 during the recent "digital" years (Figure 1a). The larger number of recently recorded events per unit time is definitely related to the great advantage of digital recording of sea level oscillations, as well as to much higher time resolution and precision of modern instruments.

Over the 1910 to 2022 period, 39 tsunamis were recorded at Victoria: 17 during 1910-1999 and 22 during 2000-2020 (Figure 1b). The high-resolution digital tide gauge installed in Victoria Harbour in the late 1990s enables us to obtain much more complete and precise tsunami statistics for this site. Examination of the statistics indicates that the maximum tsunami trough-to-crest wave heights recorded at Victoria exceeded the 20-cm threshold line[1] (denoted by a solid horizontal *red line* in Figure 1b) only for seven major events:

[1] Historically, the main parameter characterizing a tsunami event was a *trough-to-crest tsunami wave height.* This specific parameter was used to describe major historical tsunami events on the coast of British Columbia [cf. *Wigen and White*, 1960; *Wigen*, 1983]. Before 2007, ≈≈the same parameter was used in various catalogues and by the International Tsunami Warning Service (ITWS): https://ntwc.ncep.noaa.gov/recent_tsunamis/, in particular, to describe the most catastrophic tsunami event, the 2004 Sumatra tsunami, affecting the coasts of the entire World Ocean: https://ntwc.ncep.noaa.gov/previous.events/?p=12-26-04. Figure 1 shows the tsunami wave heights. However, since 2007, a *zero-to-peak tsunami amplitude* began to be commonly used for tsunamis because: (1) it is easier to estimate this parameter in digital and open-ocean tsunami records, as well as (2) in the results of numerical simulations of tsunami waves; and (3) this parameter is more important for estimation of tsunami risk, i.e., the vertical onshore inundation. The maximu tsunami wave amplitude is ≈ 1/2 of the maximum tsunami wave height. Nevertheless, quite often the terms "tsunami wave height" or "tsunami height" are used for tsunami amplitudes, without any indication that this is actually measured "zero-to-peak". This can create considerable confusion and affect the final results.

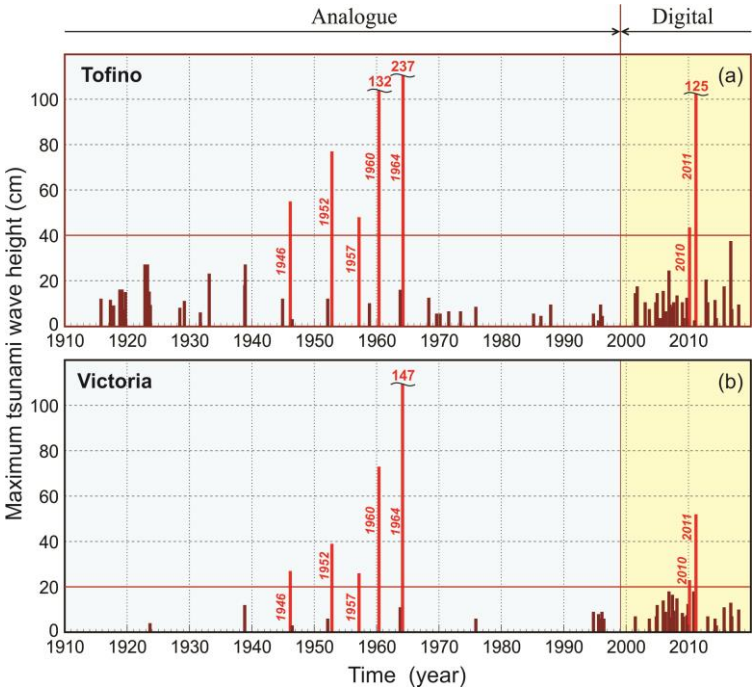

Figure 1. Maximum trough-to-crest wave heights of tsunamis recorded at (a) Tofino and (b) Victoria during the period 1910–2019. Up to 1997, measurements were made by analogue tide gauges; since July 1997, digital tide gauges have been used. Red bars indicate tsunami wave heights for the five great tsunamis of the 20th century (1946, 1952, 1957, 1960 and 1964) and two of the 21st century (2010 and 2011); all the others are indicated by magenta bars.

(1) 1946 Aleutian Islands (M_w 8.6);

(2) 1952 Kamchatka (M_w 9.0);

(3) 1957 Aleutian Islands (M_w 8.6);

(4) 1960 Chile (M_w 9.5);

(5) 1964 Alaska (M_w 9.2);

(6) 2010 Chile (Maule) (M_w 8.8);

(7) 2011 Tohoku (East Japan) (M_w 9.1).

All other trans-oceanic tsunamis recorded at Victoria were significantly weaker.

At Tofino, only the same seven major tsunamis exceeded the 40-cm threshold (denoted in Figure 1a by the *red* horizontal *line*), while all other tsunamis were much smaller. The results of this analysis clearly demonstrate that only tsunamis associated with major trans-oceanic events (earthquakes with $M_w \geq 8.6$) generate substantial wave heights at Victoria and Tofino (as well as the other BC stations). The epicenters of the seven earthquakes are indicated in Figure 2 by red stars; they are located in

three distinct regions - (1) Aleutian-Alaska; (2) Kamchatka-Japan; and (3) Chile – located to the (1) northwest, (2) west and (3) south relative to the coast of Vancouver Island (Figure 2). Tsunamis generated in other seismically active regions (Mexico/Central America, New Zealand, Samoa, Kermadec, Tonga, Philippines, etc.) are not dangerous for Vancouver Island and, in general, for the entire coast of British Columbia.

Figures 3-5 show the tsunami records for Tofino and Victoria for the seven major events listed above. In addition, for three events (1957, 1960 and 1964), the tsunami records at Fulford Harbour[2], the station that was in operation during these events, are also presented in these figures. To construct these plots, all original paper records for 1946, 1952, 1957, 1960 and 1964 events were carefully hand-digitized. All records, including the digital records of the 2010 and 2011 events, were then de-tided (i.e., the predicted tides were subtracted from the initial records).

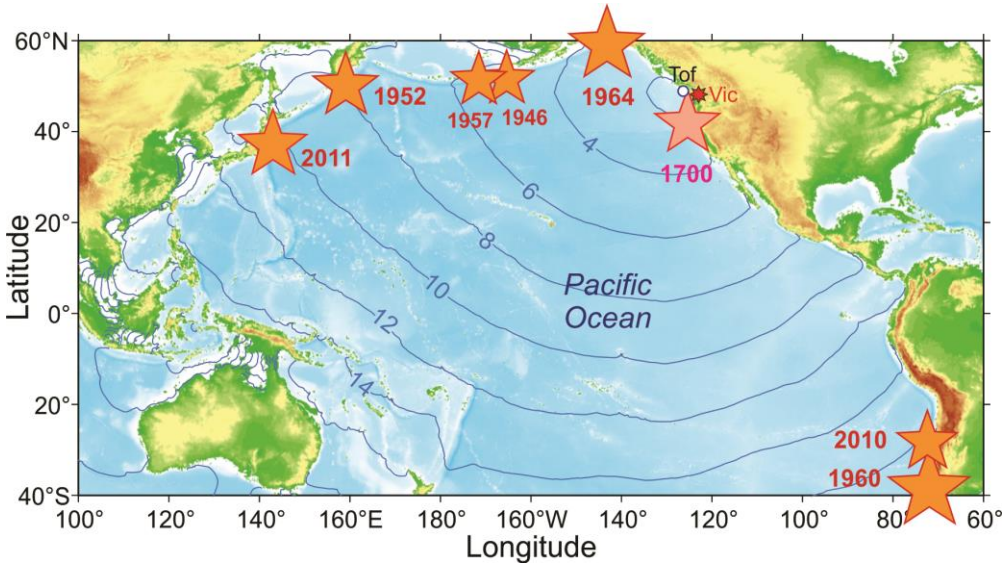

Figure 2. Epicenters (orange stars) of the five great earthquakes of the 20th century (1946 Aleutian Islands, 1952 Kamchatka, 1957 Andreanof Islands., 1960 Chile and 1964 Alaska) and the two of the 21st century (2010 Chile and 2011 Tohoku) in the Pacific Ocean that produced major trans-oceanic tsunamis. The size of the star is proportional to the earthquake magnitude (M_w). The solid blue lines are inverted isochrones of the tsunami travel time (in hours) from various parts in the Pacific Ocean to Tofino ("Tof"), British Columbia (denoted by the *white circle*). The epicenter of the 1700 Cascadia Subduction Zone earthquake is denoted by the pink star. The multibeam red star indicates the location of Victoria ("Vic").

[2] The Fulford Harbour tide gauge is located on the southern coast of Salt Spring Island in the Strait of Georgia.

The de-tiding procedure is crucial for the correct estimation of the tsunami parameters (in particular, the trough-to-crest tsunami wave heights). This procedure is illustrated by Figure 5 for the 1964 Alaska tsunami. Figure 5a shows the original records at Tofino, Victoria and Fulford Harbour (with tides), while Figure 5b presents the same records with the tides subtracted. Figure 5a indicates the importance of the tide height at the time of the event, with high tide at Tofino adding about 3 m to the tsunami compared to low water; for Victoria, the addition is about 1.5 m.

For all displayed events, tsunami waves at Tofino (i.e., on the outer open-ocean coast) are substantially higher than at Victoria at the head of Juan de Fuca Strait, while those at Victoria are higher than at Fulford Harbour in the southern Strait of Georgia. Trans-oceanic tsunami waves arriving from the open ocean attenuate in Juan de Fuca Strait and further weaken when they arrive in the Strait of Georgia.

Parameters of the seven great tsunamis recorded at Tofino and Victoria can be used to estimate empirical relationships between observed maximum tsunami trough-to-crest wave heights and arrival times for the two stations [*Rabinovich et al.*, 2019]. As shown in Figure 6, the mean ratio of maximum tsunami wave heights at Victoria versus those at Tofino, $H_{\mathrm{Vict}}/H_{\mathrm{Tof}} \approx 0.57 \pm 0.03$ (N=7), where N is the number of the events, is well constrained. Similarly, the mean square correlation coefficient, R^2 = 0.89, among events is very high (Figure 6a). As a consequence, the maximum tsunami wave height expected at Victoria will almost invariably be roughly half that for Tofino. The situation with arrival times is more complicated. In this case, the time differences (specifically, the lead time at Tofino relative to Victoria) depends on the source location. Tsunami waves arrived at Tofino and Victoria from three different directions: (1) NW (Aleutian-Alaska); (2) west (Japan-Kamchatka) and (3) south (Chile). In Figure 6b, the three regions are indicated by source-region specific symbols: Maximum time differences arise when the tsunami waves arrive from the northwest, while minimum time differences occur when the waves arrive from the south. The mean values for the three source regions are: (1) 69 min; (2) 62 min; and (3) 34 min. These estimates show that Tsunami Warning Station (TWS) Tofino can be effectively used to forecast tsunami waves at Victoria. For tsunami sources located near the coast of South America, the lead time will be a little more than 30 min, while for sources located near Alaska, the Aleutian Islands, the Kamchatka, Kuril Islands and Japan, it will be ~60-70 min [*Rabinovich et al.*, 2019].

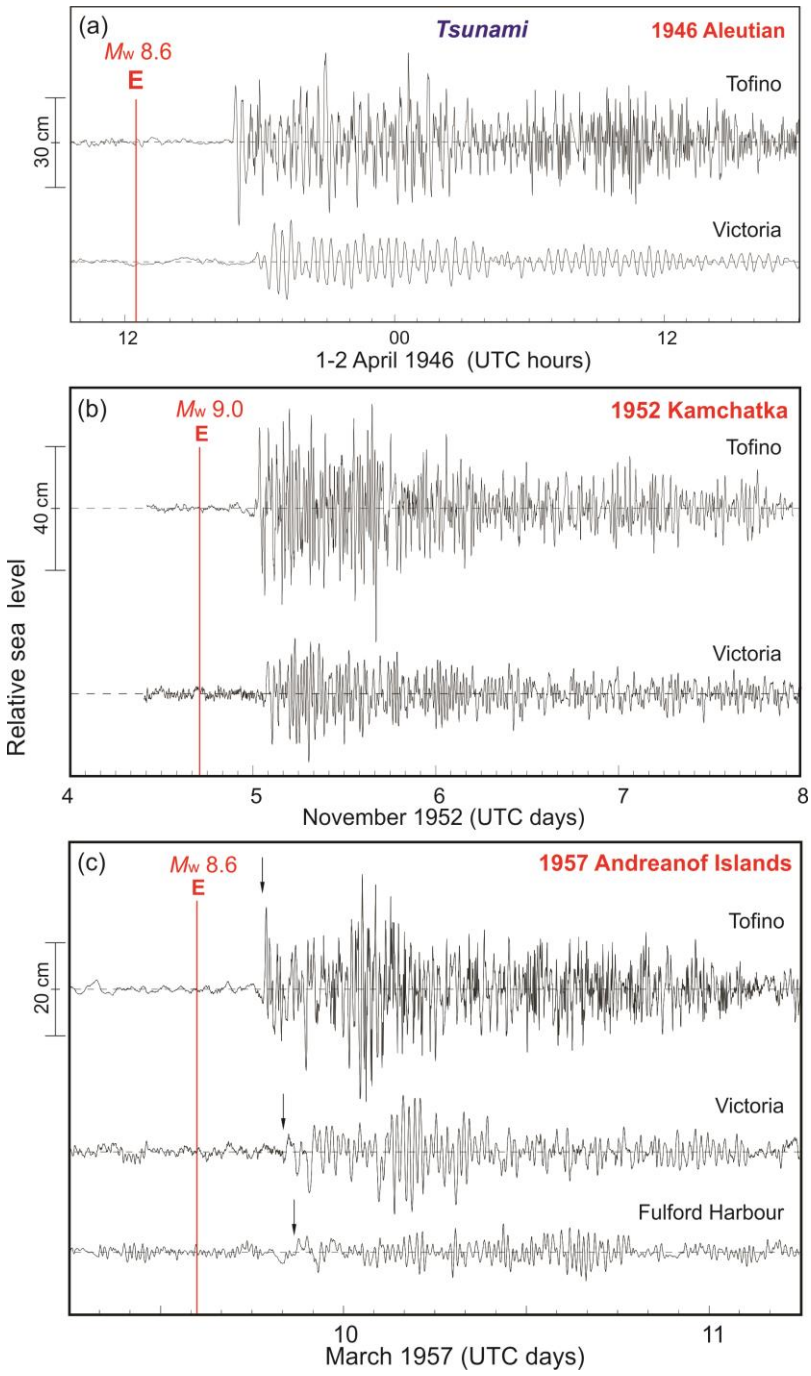

Figure 3. (a) The 1 April 1946 Aleutian tsunami recorded at Tofino and Victoria; (b) the 4 November 1952 Kamchatka tsunami recorded at Tofino and Victoria; and (c) the 9 March 1957 Andreanof Islands tsunami recorded at Tofino, Victoria and Fulford Harbour (Salt Spring Island). The solid vertical red line labelled "E" denotes the times of the earthquake; the arrows in (c) indicate the tsunami arrival times (modified from *Rabinovich et al.* [2019]).

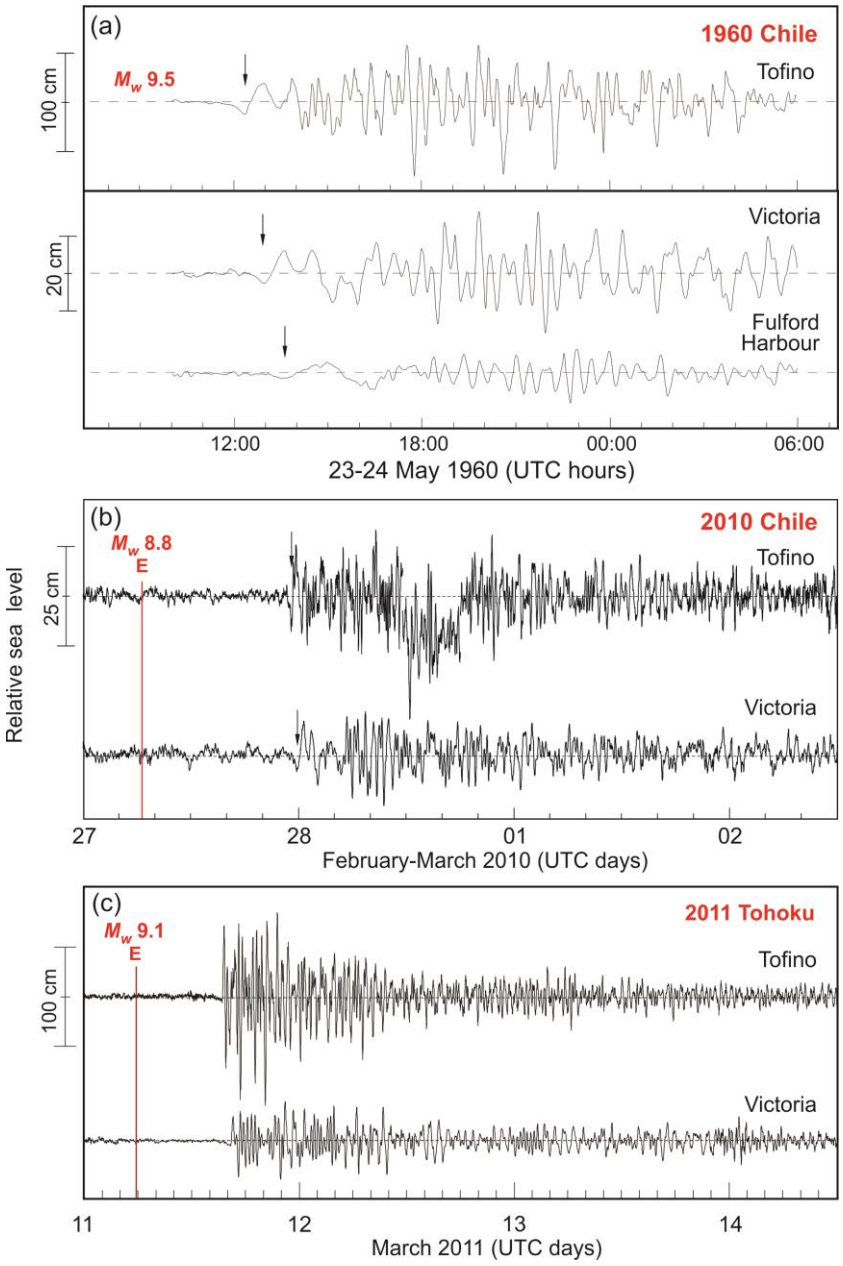

Figure 4. (a) The 22 May 1960 Great Chile Tsunami recorded at Tofino, Victoria and Fulford Harbor (modified from *Rabinovich et al.* [2019]); (b) the 27 February 2010 Chile tsunami digitally recorded at Tofino and Victoria; and (c) the 11 March 2011 Tohoku (East Japan) tsunami digitally recorded at Tofino and Victoria. The negative denivelation ("trough wave") preceding the arrival of the frontal tsunami waves for all three events is related to the elasticity of the Earth's core deflecting under the weight of the propagating tsunami wave (see details in *Watada et al*., 2014; *Eblé et al*., 2015). The arrows in (a) and (b) indicate the tsunami arrival; the solid vertical red line labelled "E" in (b) and (c) denotes the time of the 2010 Chile (M_w 8.8) and 2011 Tohoku (M_w 9.1) earthquakes, respectively; the main shock of the 1960 Chile earthquake (M_w 9.5) occurred at 19:11 UTC on 22 May.

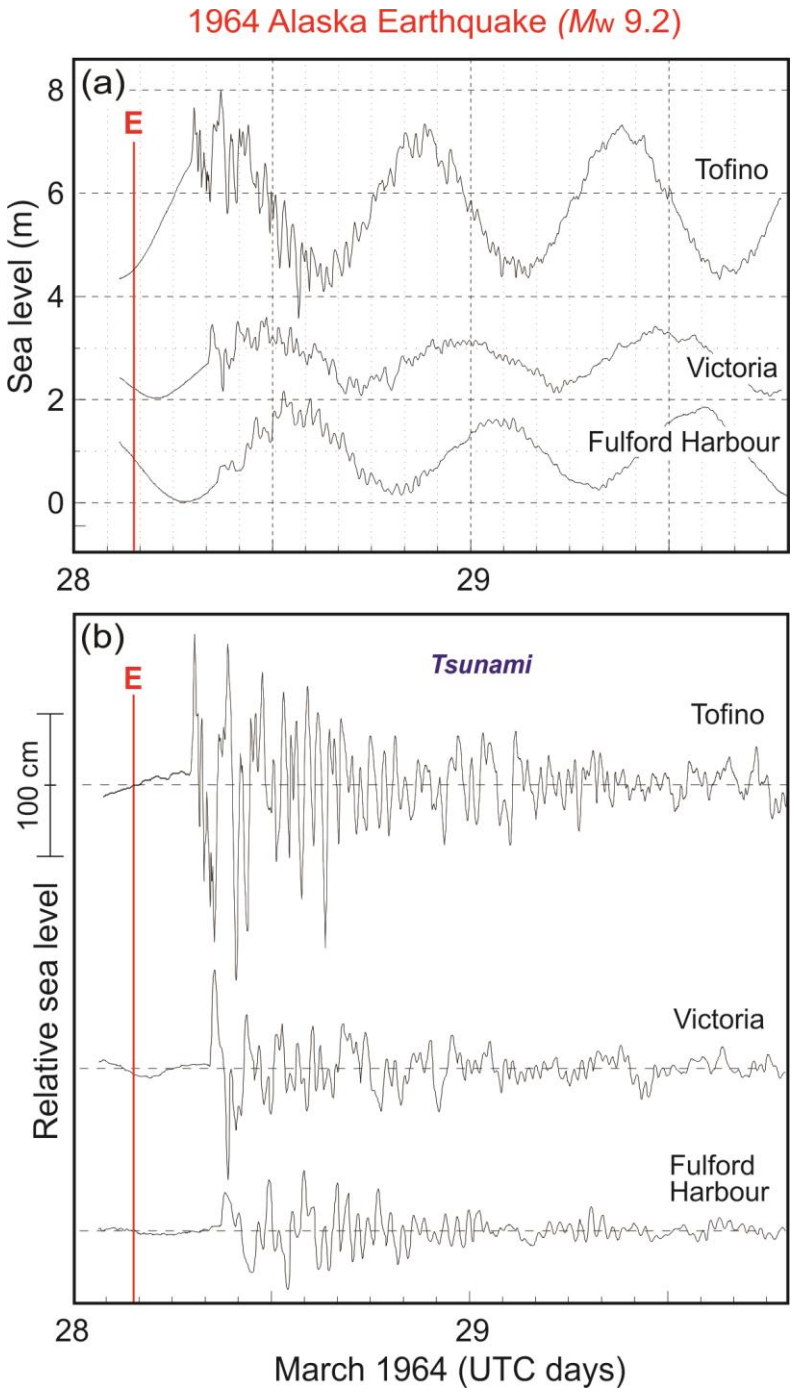

Figure 5. (a) The 28 March 1964 Alaska tsunami, including tides, as recorded at stations Tofino. Victoria and Fulford Harbour For display purposes, the records have been vertically shifted relative to each other, and (b) the same records but de-tided (residual). The solid vertical red line labelled "E" denotes the time of the earthquake. (Modified from *Rabinovich et al.* [2019]).

The strongest of all tsunamis observed on the coast of British Columbia, was the 1964 Great Alaska tsunami. This was the only tsunami that produced tsunami wave height of more than 2 m at Tofino (2.37 m) and more than 1 m at Victoria (1.47 m) (Figure 1). This specific tsunami initiated the severest damage along the BC coast (mostly at Port Alberni and Prince Rupert [*Rabinovich et al.*, 2019]). It is evident that 1964-type tsunamis potentially present the greatest danger for the Victoria area, including the Victoria Coast Guard Station. Therefore, based on modelling results of *Fine et al.* [2018a], we consider the corresponding threat, taking into account the climatic and tectonic sea level changes in this region.

The other region of attention is the Cascadia Subduction Zone (CSZ), which is a convergent plate boundary that stretches from central Vancouver Island (Canada) to Northern California (USA). The Great CSZ earthquake of 26 January 1700, with an estimated magnitude M_w 9.0, generated a major trans-oceanic tsunami that caused significant destruction in Japan, on the opposite side of the Pacific Ocean [cf. *Atwater et al.,* 2005], and strongly affected the outer coast of British Columbia. In Figure 2, the epicenter of the 1700 CSZ earthquake is indicated by a pink star. There is no reliable information on historical heights on the coast of British Columbia associated with this tsunami, however, paleotsunami findings on the coast of Vancouver Island [cf. *Clague et al*., 2000, 2003] show that tsunami waves of ~15 m likely struck the outer coast of the island at the time of the 1700 earthquake and that the waves also penetrated into Juan de Fuca Strait and the Strait of Georgia. We briefly consider the modelling results of *Fine et al*. [2018b] for the 1700 CSZ-type tsunami for the Victoria area and the influence of sea level change on the corresponding wave height estimates.

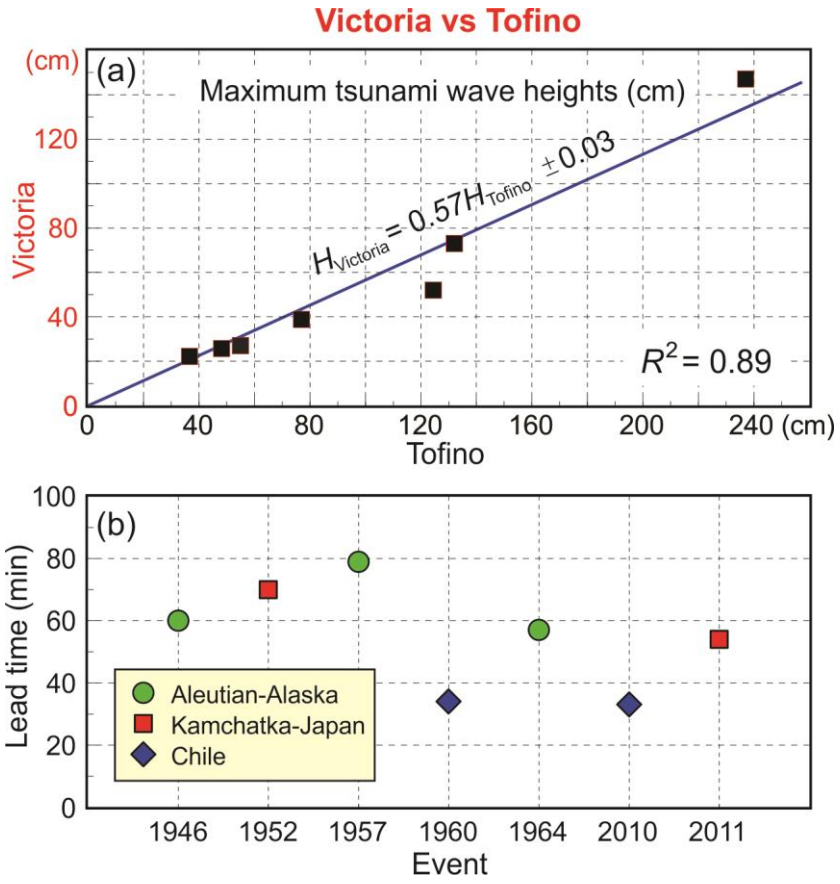

Figure 6. (a) Empirical relationship between the maximum trough-to-crest tsunami wave heights at Victoria vs Tofino for the seven great events (1946, 1952, 1957, 1960, 1964, 2010 and 2011). (b) The difference in tsunami arrival times ("lead time") between Tofino and Victoria for the three groups of source regions: Aleutian-Alaska (1946, 1957 and 1964); Kamchatka-Japan (1952 and 2011); and Chile (1960 and 2010). (Modified from *Rabinovich et al.* [2019]).

3 MODELLING MAJOR TSUNAMIS FOR THE AREA OF VICTORIA

Based on all findings and on preliminary numerical modeling results, *Fine et al.* [2018a,b] concluded that the major threat for the area of Victoria are associated with great tsunamis generated in two specific source regions that actually are the closest to the coast of British Columbia: (1) Alaska (a 1964-like event) and (2) the Cascadia Subduction Zone (a 1700-like event), while other tsunami-source regions may be ignored. Their numerical studies provide estimates of the expected maximum tsunami wave amplitudes arising from these two types of events.

A high-resolution, nested-grid tsunami model was used by *Fine et al.* [2018a,b] to simulate the distribution of tsunami waves and wave-induced currents. The model is based on a finite-difference formulation of the linear shallow-water equations and is similar to that of *Imamura* [1996] and to the one by *Fine et al.* [2013, 2015] for numerical modelling of the 2011 Tohoku and 2012 Haida-Gwaii tsunamis.

3.1. Nested grids

Accurate numerical simulation of tsunami waves in the rapidly shoaling regions of the west coast of British Columbia requires setting up the model domain as a series of nested grids of ever finer spatial and temporal resolution. The use of nested grids of smaller cell dimensions and time steps makes it possible to resolve tsunami wave configurations as they propagate into the shallow coastal regions. A good interface between the inner and outer domains is required to avoid errors and model instability associated with point matching between the different grids. High resolution bathymetry, external forcing and observations are needed for model domain setup, initialization and validation at each domain level. In their numerical simulations of the 1964-like Alaska and 1700-like CSZ tsunamis, *Fine et al*. [2018a, b] fulfilled all these requirements and used the nested-grid formulation similar to that one in well-known tsunami models, TUNAMI and COMCOT [*Liu et al.*, 1998; *Imamura et al.*, 2006].

For both projects (1964 Alaska and 1700 CSZ), *Fine et al*. [2018a, b] used a series of four nested grids; Grid 3 and Grid 4 were the same for both projects, while Grid 1A and 2A for the 1964 Alaska project were different from Grid 1B and 2B for the 1700 CSZ project (Table 1). The choice of model grids took into account the need for high spatial resolution to accurately resolve the reflection and transformation of the tsunami waves.

Grid 1A is the coarsest numerical grid used in the 1964-like Alaska model; it covers the northeast Pacific and encompasses the major source region used in the simulations, the Alaska Fault or failure Zone (Figure 7a). The spatial resolution of the grid is 30 arc-seconds in both the east-west direction (spatial scales in the *x*-direction are 0.45 km to 0.7 km, depending on latitude) and the north-south direction (0.9 km *y*-direction grid size). The grid is bounded by 45 – 62° N, 157 – 122° W. Grid 1B covers the northeast Pacific and encompasses the major source region used in the simulations for, the Cascadia Subduction Zone (CSZ) (Figure 7b). The spatial resolution of the coarse grid is 90 arc-seconds in the east-west (*x*) direction (spatial scales ranged from 1.4 km to 2.2 km, depending on

latitude) and 45 arc-seconds in the north-south (*y*) direction (1.4 km grid size). The grid is bounded by 38– 55° N, 140 – 122° W. A typical spatial scale for each grid cell is thus about 1.5 km. Both grids were created using the 30 arc-second global bathymetry dataset GEBCO2014 (GEBCO, 2014).

Table 1: Parameters of the numerical grids used in the tsunami generation and propagation models. Grid extent is along the *x* (eastward) and *y* (northward) coordinate directions and is presented in latitude and longitude degrees (°). Numerical grid cell sizes for Grids 2A, 2B, 3 and 4 are roughly 185, 278, 46 and 10 m, respectively.

Grid No.	Extent (*x*, *y*; degrees)	Array (number of grid points)	Cell size (*x*, *y*; degrees)	Source of data	Processing type
1A	34.0, 16.0 (1964, Alaska)	4081, 1921	0.00833, 0.00833	GEBCO 2014 30 arc- seconds gridded data	None
1B	18.0, 17.0 (1700, CSZ)	720,1361	0.025, 0.0125	GEBCO 2014 30 arc- seconds gridded data	Filtering and bilinear interpolation
2A	6.8, 4.235 (1964, Alaska)	4081,2542	0.0016667, 0.0016667	BC Coastal Relief, 3 sec; US Coastal Relief, 3sec	Filtering and bilinear interpolation
2B	2.45, 1.95 (1700, CSZ)	589,780	0.00416667, 0.0025	BC 3 arc-sec bathymetric DEM	Filtering and bilinear interpolation
3	0.22167, 0.21	291, 506	0.0008333, 0.00041667	BC Coastal Relief, 3 sec CHS bathymetry data	Filtering and bilinear interpolation
4	0.12217, 0.0765	740, 920	0.000166667, 0.0000833	CHS bathymetry data	Kriging, smoothing, bilinear interpolation

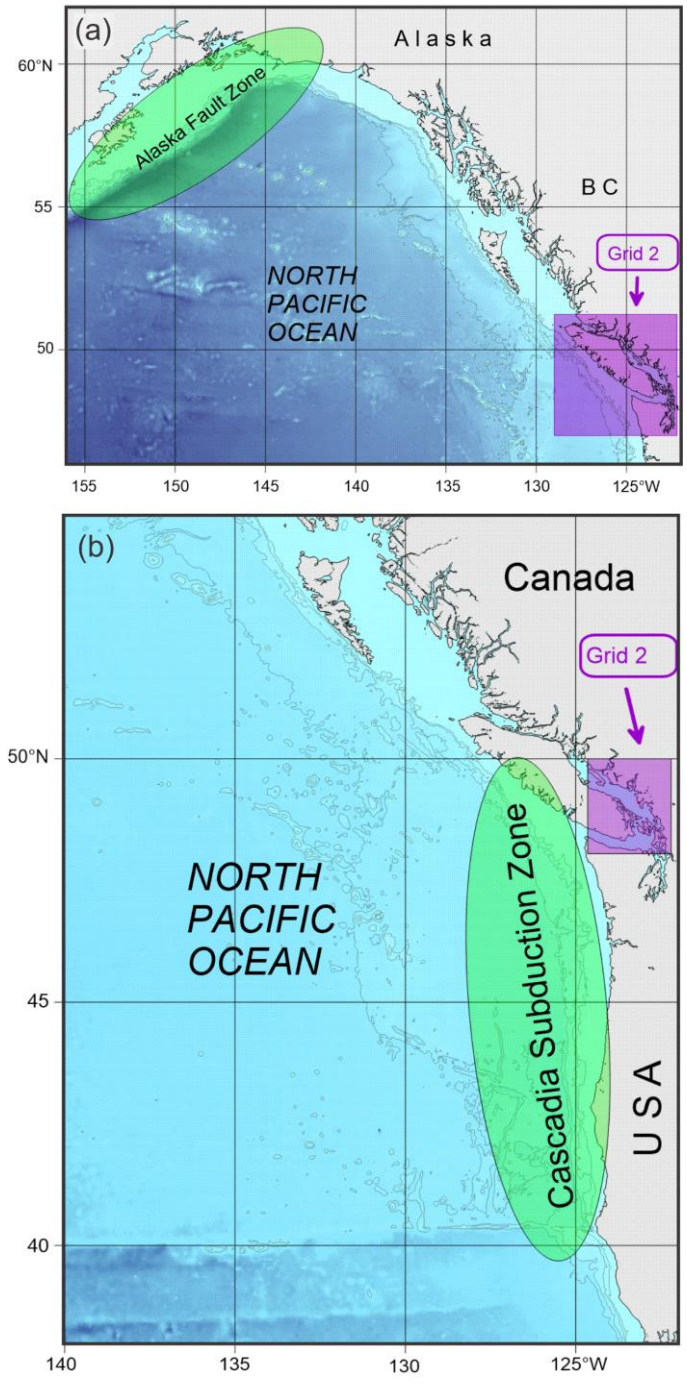

Figure 7. The regions of the northeast Pacific covered by the large-scale coarse grid numerical models. (a) Grid 1 for numerical modelling of an Alaska 1964-type tsunami. Also shown is the Alaska Fault Zone that could generate tsunamis that impact the Coast Guard facility. The location of the first nested grid (Grid 2) is shown covering the coast of Vancouver Island. (b) Grid 1 for numerical modelling of a CSZ 1700-type tsunami. Also shown is the Cascadia Subduction Zone where a tsunami could be generated that would impact the Victoria Coast Guard facility. The inset shows the location of the first nested grid (Grid 2), covering the southwest coast of British Columbia. (Modified from *Fine et al.* [2018a,b]).

Grid 2A used for the 1964-like Alaska model covers southern British Columbia, including the shelf of Vancouver Island and the surrounding waters, and the northwest US Coast (Figure 8a). The northern part of the grid was created using the British Columbia 3 arc-second Digital Elevation Model (NOAA, 2017); the southern part was created using the 3 arc-second US Coastal Relief. Grid 2A has a resolution of 6 arc-seconds in both the east-west direction and in the north-south direction, corresponding to spatial scales of approximately 125 m and 185 m, respectively (Table 1). The grid spans the northern coast with boundaries of 47 – 51°N, 129 – 122°W. Grid 2B covers southern northwest British Columbia and the northwest US coast (Figure 8b). It extends equally to the west and to the east of the Victoria region and also covers the shelf region. This grid was used in the 1700-like CSZ model. Grid 2B has a resolution of 15 arc-seconds in the east-west direction and 9 arc-seconds in the north-south direction, corresponding to spatial scales (x, y) of approximately 270 m and 280 m, respectively (Table 1). The grid boundaries span 48.2 – 50°N, 124.5 – 122°W.

The third numerical grid (Grid 3) covers the southern end of Vancouver Island near Victoria and the surrounding passes and inlets of Juan de Fuca Strait (Figure 9); it was used both for the 1964-like Alaska and 1700-like CSZ models. This grid is of considerable importance since it determines the transformation of the incoming waves in the vicinity of Victoria. Model grid cells were created using the British Columbia 3 arc-second bathymetric DEM (2017). The gridded data were subsequently re-interpolated to a geographical coordinate system (NAD83 standard) with a rectangular grid-cell size of 3 arc-seconds by 1.5 arc-seconds (approximately 61 m by 46 m) in the east-west and north-south directions, respectively.

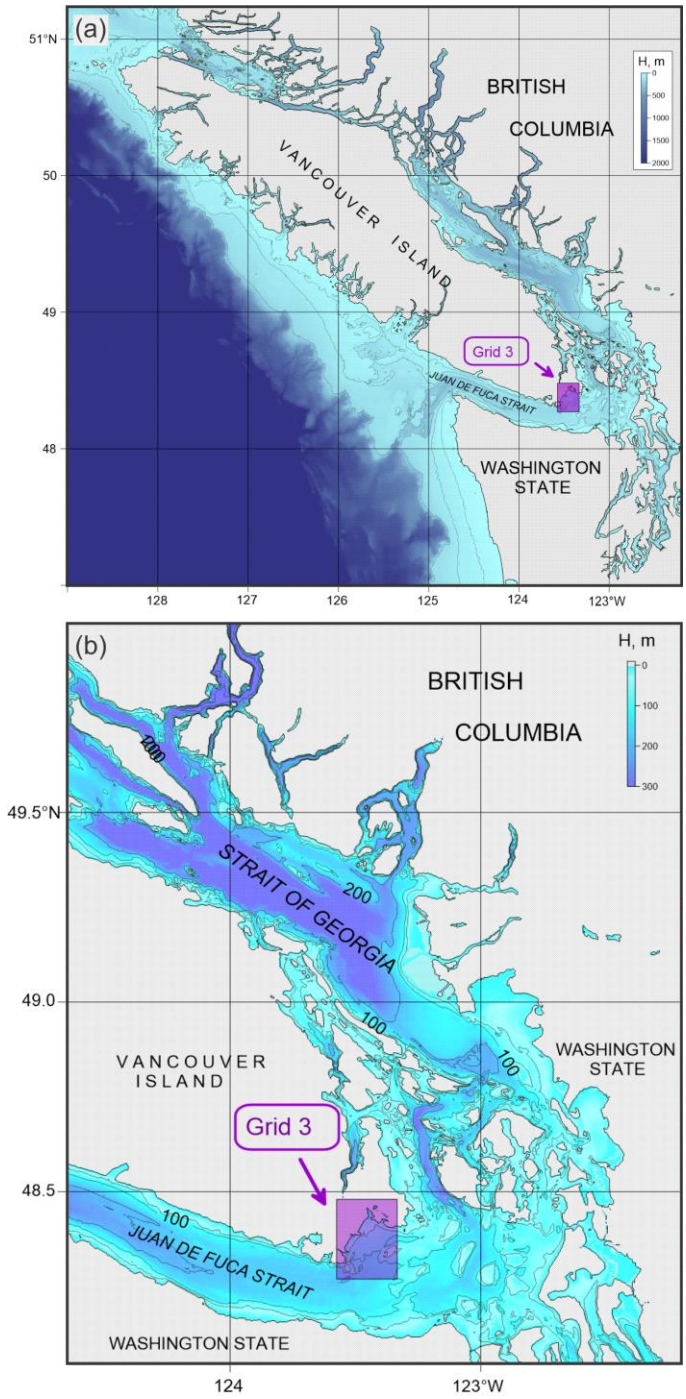

Figure 8. (a) The region covered by the medium-scale bathymetric grid (Grid 2) for the Vancouver Island and Washington State coasts. The horizontal (x, y) grid cell scales for this region are approximately 125 m and 185 m, respectively. (b) The Salish Sea region covered by the medium-scale bathymetric grid (Grid 2) for the southwest coast of British Columbia. The horizontal grid cell scales (x, y) for this region are approximately 270 m by 280 m, respectively. The insets in (a) and (b) show the boundaries and location of the second nested grid (Grid 3) covering the region of Victoria. Depths, H, are in metres (m). (Modified from *Fine et al.* [2018a,b]).

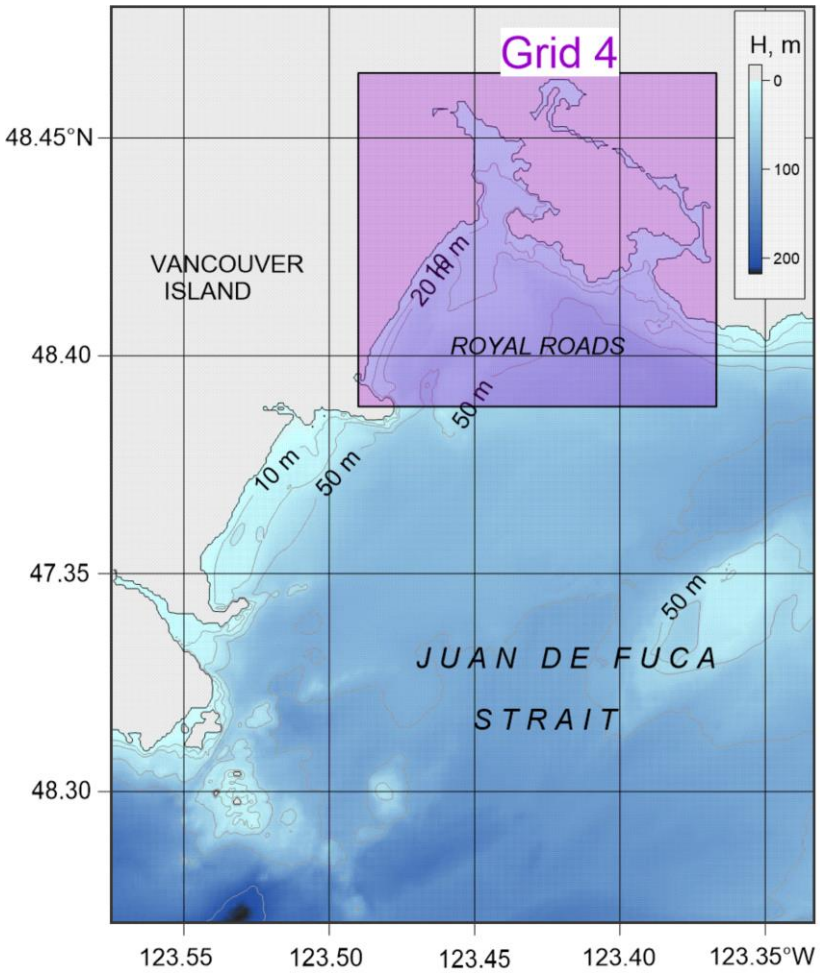

Figure 9. Coastal region covered by Grid 3, southern Vancouver Island coast and eastern Juan de Fuca Strait. The grid scale for this region is approximately 61 m by 46 m. The inset shows the boundaries and location of the fourth nested grid (Grid 4) covering Esquimalt and Victoria harbours. Depths are in metres (m). (From *Fine et al.* [2018a,b]).

The final (fourth) numerical Grid 4 was also used both for the 1964-like Alaska and 1700-like CSZ models. It has the highest spatial resolution and covers coastal areas in Victoria (Figure 10). The grid encompasses both Victoria and Esquimalt harbours and is designed specifically for estimations of tsunami inundation and tsunami-induced currents in the vicinity of the Coast Guard facilities. A Kriging algorithm (see details of the algorithm in *Thomson and Emery* [2014]) was used to create the grid from the original, irregularly-spaced bathymetric data. The high-resolution grid (x, y) scale is approximately 12 m by 9 m; the bathymetry was adjusted around Victoria Harbour to account for changes in depth between the shoreline bathymetry at the time of the 1964 event and at present.

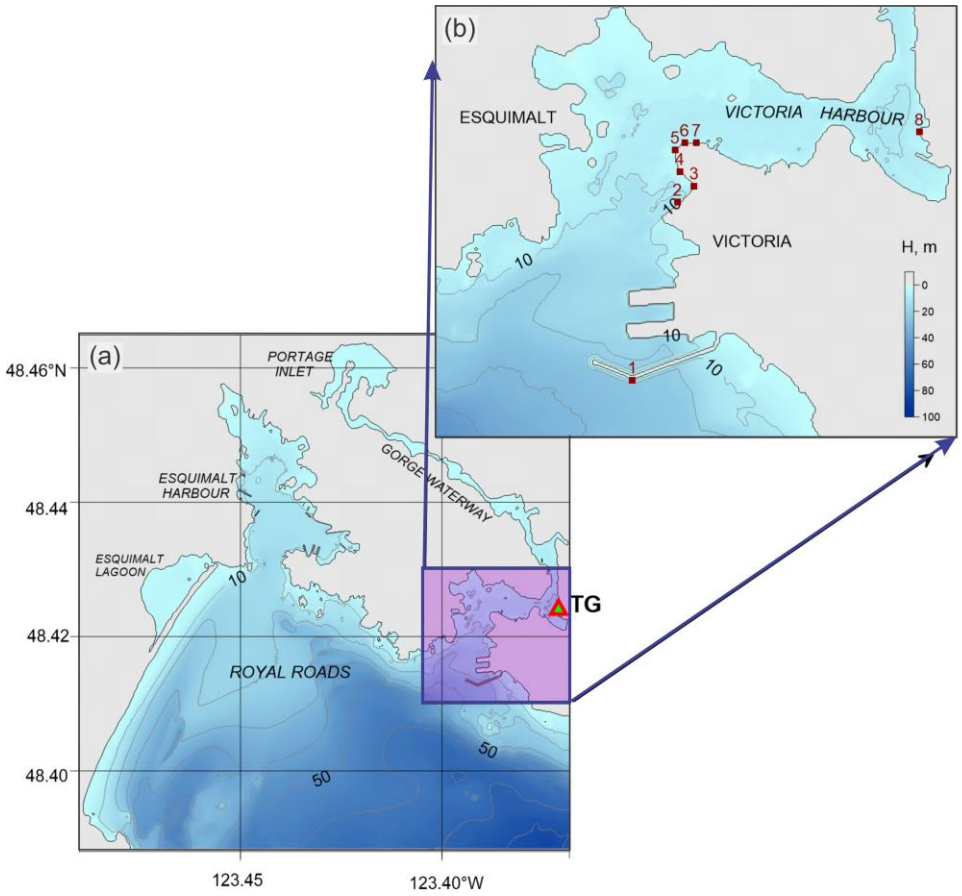

Figure 10. (a) The region covered by Grid 4; the fine-scale bathymetric grid has adjusted topography for the region of Victoria Harbour, and has a grid (x, y) scale of approximately 12 m by 9 m. (b) The location of the Victoria tide gauge (TG) and the sites (1-8) within the Victoria harbour for which tsunami waveforms were simulated. Depths are in metres (m). (Modified from *Fine et al.* [2018a,b]).

3.2. Modelling a 1964-type Alaska tsunami

The momentum magnitude (M_w) 9.2 Alaska earthquake of 28 March 1964 produced a catastrophic tsunami, the second strongest in the 20th century (after the magnitude 9.5 1960 Chilean tsunami). The maximum water rise was 20 m at the source and the event generated the strongest tsunami response ever observed on the coast of British Columbia [cf. *Rabinovich et al.*, 2019]. The 1964 earthquake occurred within the Alaska-Aleutian megathrust zone, where the Pacific Plate subducts under the North American Plate (Figure 11). This zone has the greatest potential to generate destructive tsunamis and is one of the most seismically active fault zones in the North Pacific. The 1964 megathrust Alaska earthquake caused the most destructive tsunami in Alaskan history and,

further south, strongly impacted the west coasts of the USA and Canada [cf. *Johnson et al.*, 1996; *Lander*, 1996].

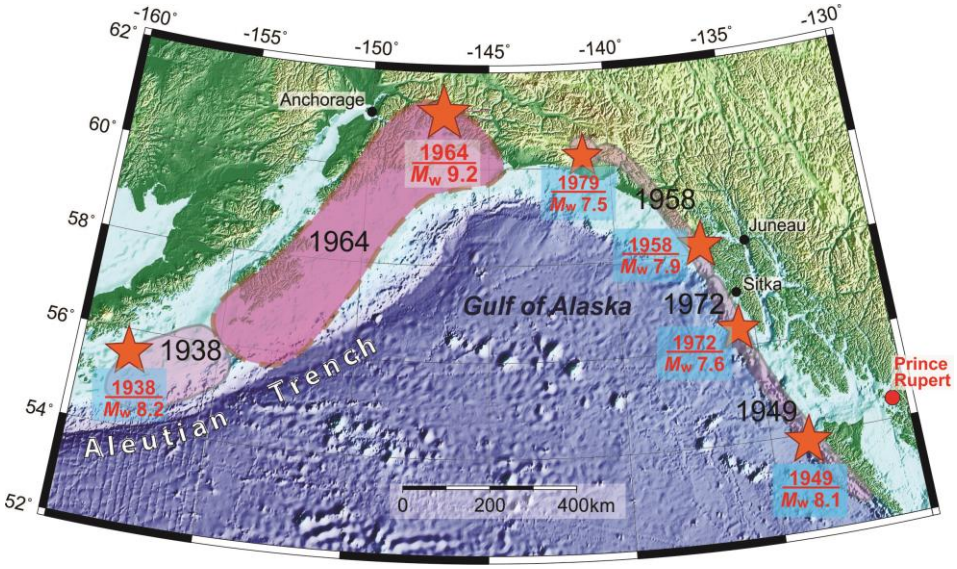

Figure 11. Map of south-central and south-eastern Alaska with the rupture zones of six major historical earthquakes (shaded); the rupture zone of the 1964 Alaska earthquake is contoured by a thick brown dashed line. Red stars indicate epicenters of the earthquakes; the sizes of the stars are proportional to the earthquake magnitudes. Tide gauges at Sitka, Juneau and Anchorage are indicated by solid black circles; the red circle denotes the tide gauge at Prince Rupert. (Modified from *Rabinovich et al.* [2019]).

The 1964 tsunami spread over the entire Pacific Ocean and was recorded by 18 instruments on the coast of British Columbia, including those in the Strait of Georgia, along the Fraser River and even in Pitt Lake [*Rabinovich et al.*, 2019]. The tsunami caused about $10 million in damage (1964-dollar values), mainly at the twin towns of Alberni and Port Alberni, with the maximum tsunami run-up at Port Alberni of about 8 m [cf. *Rabinovich et al.*, 2019].

Several numerical models were constructed to simulate tsunami wave propagation from the 1964 source, including the coast of British Columbia [cf. *LeBlond et al.*, 1989; *Dunbar et al.*, 1991; *Myers and Baptista*, 2001]. However, the models were based on preliminary source estimates and very coarse grids with 1.0-5.0-km spatial resolution. To estimate maximum possible tsunami amplitudes and tsunami-generated currents in the area of Victoria, more detailed high-resolution bathymetry, which became available recently, and a more refined source region, are needed. The 1964 Alaska tsunami is typically considered as a proxy for a major future tsunami along the Pacific coast

of North America [*Suleimani et al.*, 2013]. Therefore, to compute the expected tsunami waves for the Victoria area and, specifically, for the Victoria Coast Guard Station, *Fine et al.* [2018a] applied an Alaska 1964-type (M_w 9.2) earthquake as the tsunami source.

The numerical simulation of the 1964 tsunami was based on the newly revised [*Suleimani et al.*, 2013] coseismic slip distribution for the 1964 rupture derived from the model of *Suito and Freymueller* [2009]. The latter is a 3D viscoelastic model, which uses realistic geometry with a shallow-dipping elastic slab to describe the 1964 post-seismic deformation. *Fine et al.* [2018a] applied the inversion-based model by *Johnson et al.* [1996] as the basis for their coseismic slip model, adjusting it to the new geometry and critically reinterpreting the coseismic data. *Suleimani* [2011] used results of the near-field modelling of the 1964 tsunami to constrain the amount of slip placed on intraplate splay faults, and to evaluate the extent of the Patton Bay fault. The resulting coseismic vertical deformation is shown in Figure 12. The tsunami simulations revealed that including deformation due to horizontal displacements in the source function resulted in an increase in the far-field tsunami amplitudes.

To verify their model, *Fine et al.* [2018a] numerically simulated a tsunami waveform of the 1964 Alaska tsunami for the Victoria tide gauge site and compared the modelled results with the actual record of the tsunami (Figure 5b). Comparisons of the observed and modelled results are shown in Figure 13 and Table 2. It is evident that the modelled record fits the observed record quite well. For both the observed and simulated records, the first wave is a crest wave and is the largest wave in the records. The maximum tsunami travel times coincide within 5 minutes, indicating that they are very similar, despite the observations being based on a digitized analogue record [cf. *Rabinovich et al.*, 2019].

Table 2. Statistical properties of modelled and observed tsunami waves at the Victoria tide gauge location for the March 1964 Alaska tsunami source region. Wave amplitudes (zero-to-crest) are in metres and travel times are in hours (h) and minutes (min).

	First (maximum) wave			Visible period (min)
	Amplitude (m)	Travel time	Time of maximum elevation (UTC)	
Modelled	0.58	4h 39 min	08:15	40, 90
Observed	0.70	4h 44 min	08:20	40, 90

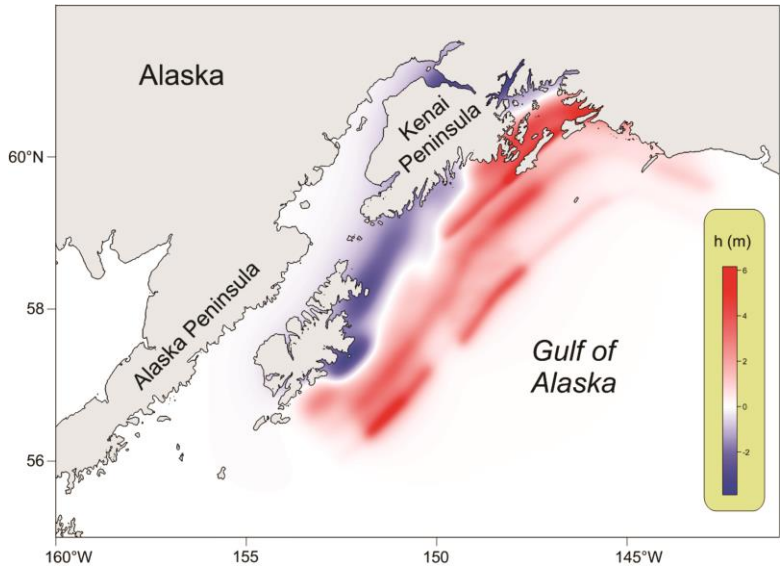

Figure 12. Seafloor vertical displacements (m) at the source region for the March 1964 Alaska tsunami. The displacements range from roughly -3 m (blue) to +6 m (red). (Modified from *Suleimani et al*. [2013]).

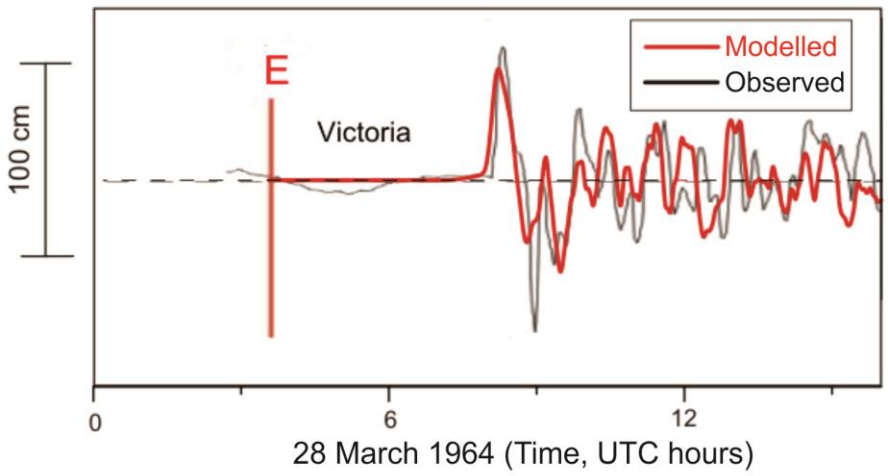

Figure 13. Observed versus modelled wave records for the March 1964 Alaska tsunami for the Victoria tide gauge site. The letter "E" denotes the time of the earthquake. (Modified from *Fine et al.* [2018a]).

The wave maxima for the 1964-type tsunami for Grids 1 and 2 computed by *Fine et al.* [2018a] are presented in Figure 14 and for Grids 3 and 4 in Figure 15. Figure 14a shows the "rays" of maximum tsunami waves for the entire northeast Pacific. The main 1964 tsunami energy flux radiated southeast toward the coast of California, but the left side of this flux affected British Columbia, in particular, the outer coast of Vancouver Island (Figure 14b). In more sheltered areas, such as Juan de Fuca Strait, the computed tsunami wave amplitudes are markedly smaller (Figure 14b; Grid 2).

Results for the finer resolution grids (Grids 3-4) demonstrate the considerable spatial variability in the incoming tsunami wave amplitudes for the study region. Figure 15a shows the distribution of the tsunami wave amplitudes for Grid 3 in eastern Juan de Fuca Strait off southeastern Vancouver Island. As the figure indicates, wave amplitudes increase toward the shoreline and are especially high in the upper reaches of Victoria Harbour, where the wave amplitudes are 3-4 times higher than in the central part of Juan de Fuca Strait. The pronounced increase in tsunami waves in Esquimalt and Victoria harbours (Figure 15b) is related to resonant amplification of the incoming tsunami waves in these harbours.

Figures 15b and 15c present high-resolution maps showing the distribution of the maximum tsunami amplitudes in Victoria Harbour and vicinity. The tsunami wave amplitudes gradually increase from the entrance to the head of the basins (for both Esquimalt Harbour and Victoria Harbour). Tsunami amplitudes at the harbour heads are almost **1 m** and are up to twice as high as those at the entrance (~0.5 m). At the Victoria Coast Guard site, the maximum tsunami wave amplitude is **0.56 m**.

Detailed analysis of the sea level variability was carried out by *Fine et al.* [2018a] for 8 sites around Victoria Harbour (Figure 15c), ranging from the outer breakwater (Site 1) to the location of the tide gauge in the inner harbour (Site 8). Figures 16a and 16b show that the simulated tsunami waves at the Coast Guard site are 5 to10% lower than those at the tide gauge site in the inner harbour (Figure 13).

There is almost no difference in the wave amplitudes at Sites 2 to 7 and all records at the Coast Guard site are nearly identical; the record at Site 8, corresponding to the tide gauge location, shows 5-10% higher wave amplitudes than at the Coast Guard sites (Figure 16). Generally, all records have nearly similar amplitudes, indicating that the spatial distances of the outer and inner parts of Victoria Harbour are short compared with the wavelengths of the incoming waves. On the other hand, when

the full harbour system is considered (including the shallow Selkirk and Gorge waters), the incoming waves are found to be significantly amplified.

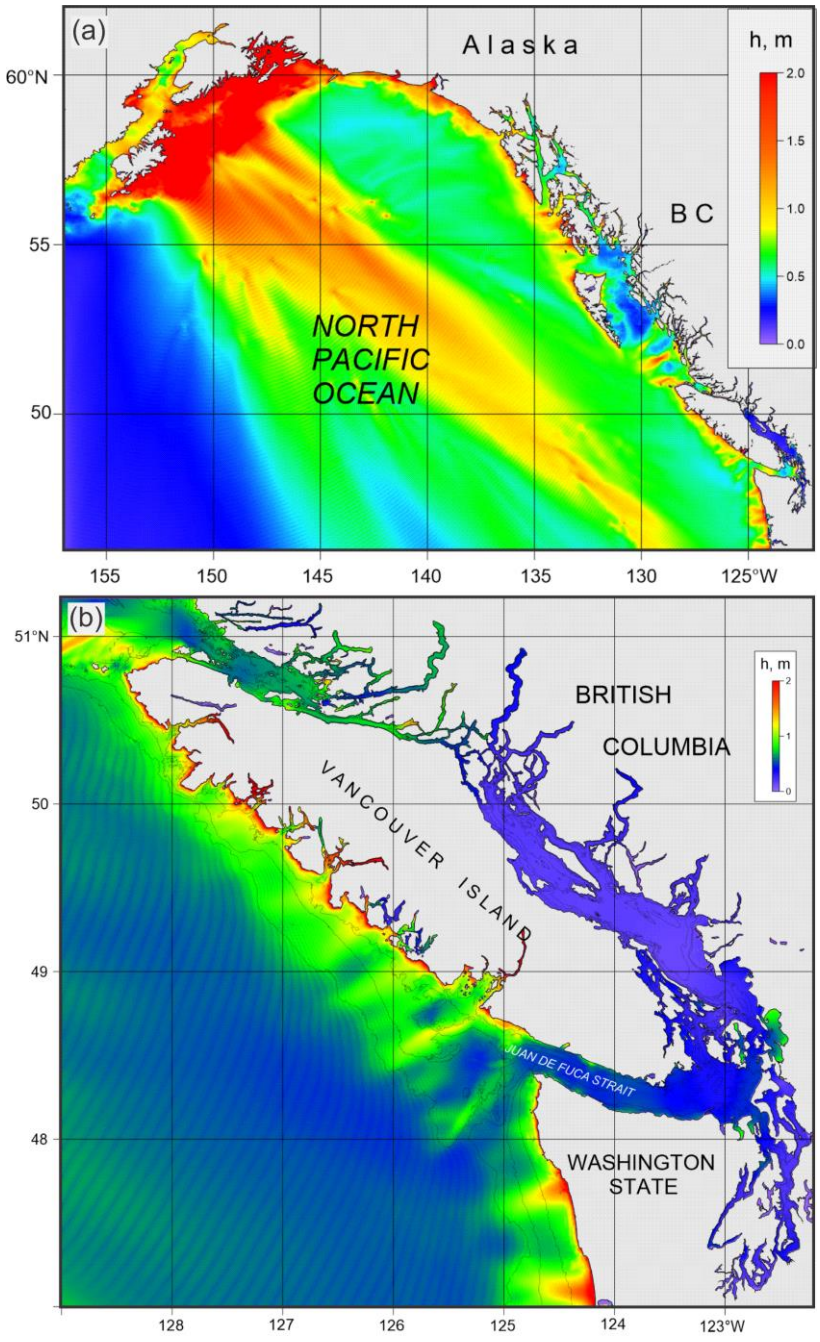

Figure 14. Distribution of maximum tsunami wave amplitudes (meters) for (a) Grid 1 and (b) Grid 2 of the nested-grid model for waves generated by simulation of the 1964 tsunami. (Modified from *Fine et al.* [2018a]).

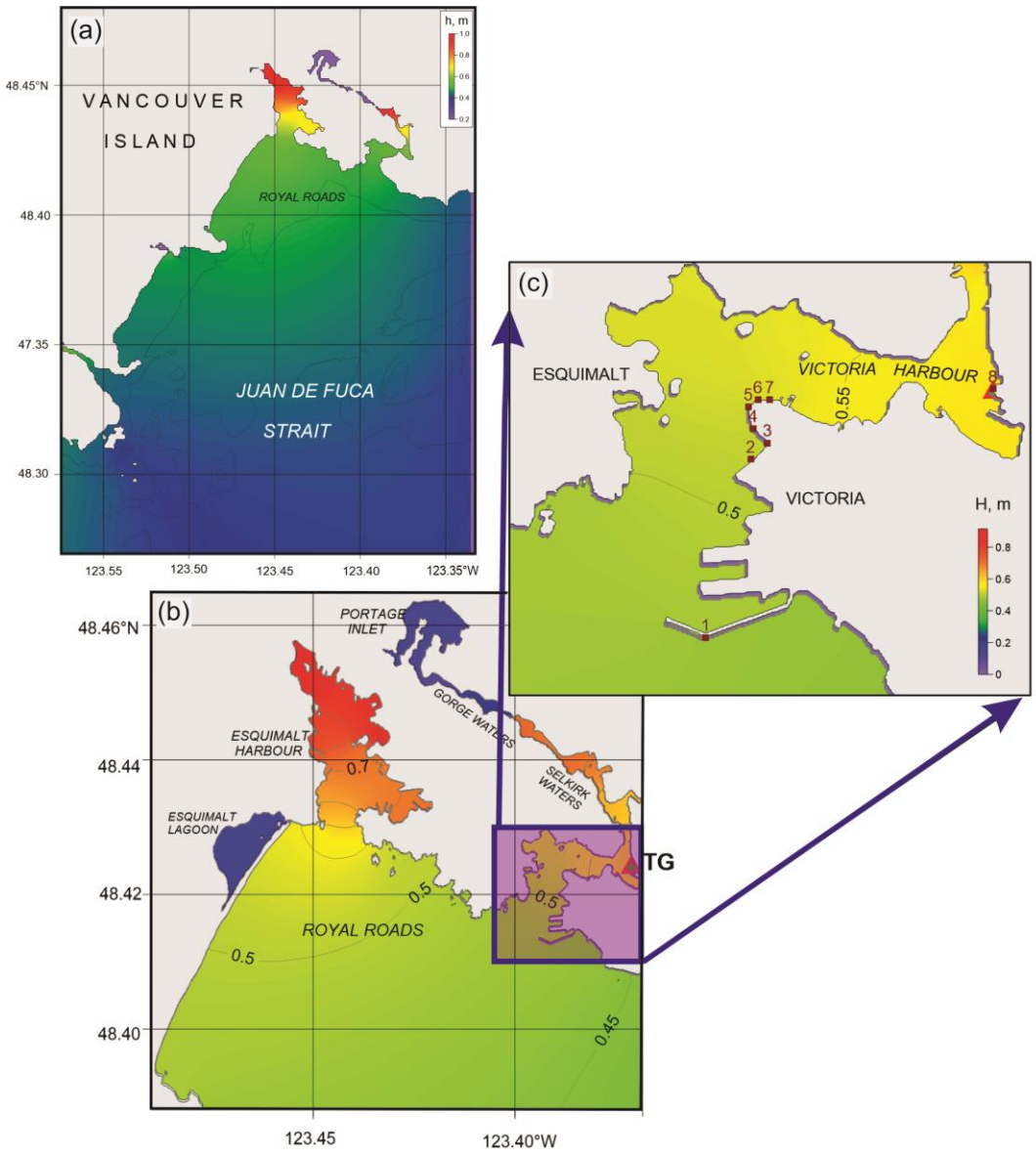

Figure 15. Distribution of maximum tsunami wave amplitudes (metres) for (a) Grid 3 and (b) Grid 4 of the nested-grid model for waves generated by simulation of the 1964 tsunami. (c) An enlarged map for Victoria Harbour with the Sites 1 to 8 marked. (Modified from *Fine et al.* [2018a]).

In general, the high-resolution, nested-grid tsunami simulation by *Fine et al.* [2018a] yielded the following principal results:

- The tsunami at the Victoria Coast Guard Facility will reach **0.56 m** above the tidal level or (0.56 m + 0.73 m) = **1.29 m** above mean sea level at the time of the wave arrivals, with the first wave being the highest wave;

• The distribution of tsunami wave amplitudes in the vicinity of the Victoria Coast Guard Facility will be nearly spatially uniform.

Because details of future possible tsunamis remain unknown in many aspects, *Fine et al.* [2018a] recommend the use of a **safety factor of 50%**, which should be added to the tsunami amplitudes estimated for a 1964-type event. Based on our analysis of the Alaska 1964 tsunami, the safety level for Victoria should be at least **0.84 m above Mean Higher High Water (MHHW)**, or **1.94 m above Mean Sea Level (MSL)**.

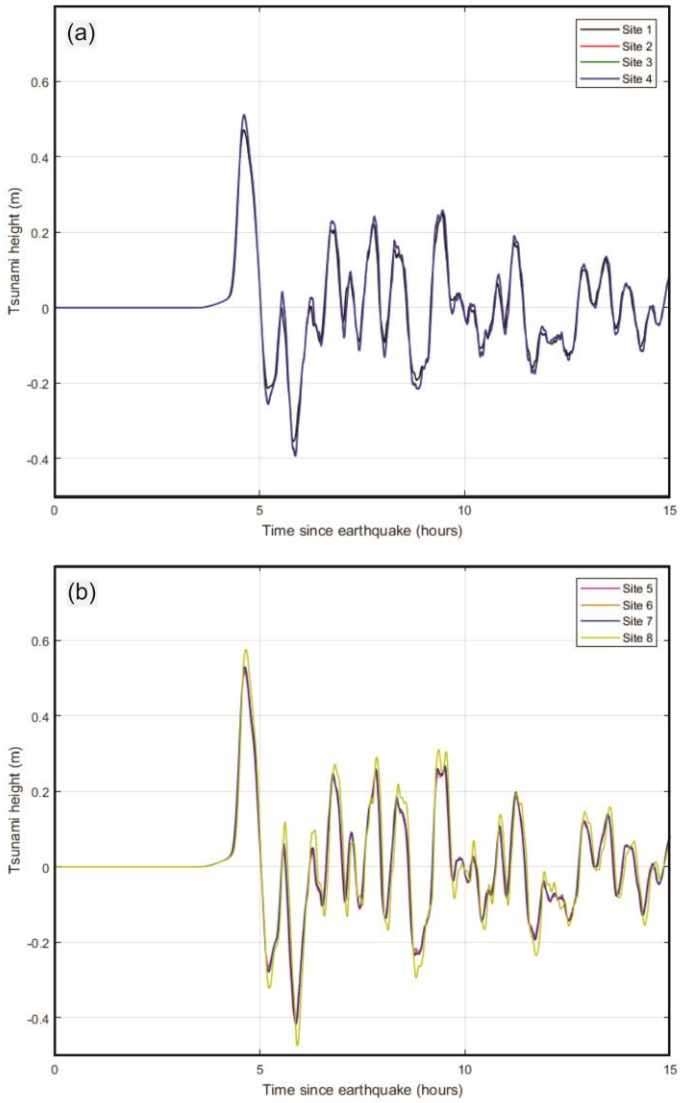

Figure 16. Simulated records of sea level variation for the Alaska 1964 tsunami at (a) Sites 1 - 4 and (b) Sites 5 – 8 within Victoria Harbour (See Figures 10b and 15c for the site locations). (Modified from *Fine et al.* [2018a]).

3.3. Modeling a 1700-type Cascadia Tsunami

The Cascadia Subduction Zone (CSZ) is a convergent plate boundary that stretches from central Vancouver Island (Canada) to Northern California (USA). It is here that the Explorer, Juan de Fuca, and Gorda plates slide eastward below the continental North American Plate (Figure 17). The Great CSZ earthquake of 26 January 1700, which had an estimated magnitude M_w = 9.0, generated a major trans-oceanic tsunami that caused significant destruction in Japan on the opposite side of the Pacific Ocean [cf. *Satake et al.*, 1996; *Atwater et al.*, 2005], and strongly affected the outer coast of British Columbia. There is no reliable information or data concerning historical heights on the coast of British Columbia associated with this tsunami, however, paleotsunami findings on the coast of Vancouver Island and the west coast of the USA [cf. *Wang et al.*, 2003; *Clague et al.*, 2000, 2003; *Wang et al.*, 2013] show that tsunami waves of ~15 m likely struck these coasts at the time of the 1700 CSZ earthquake.

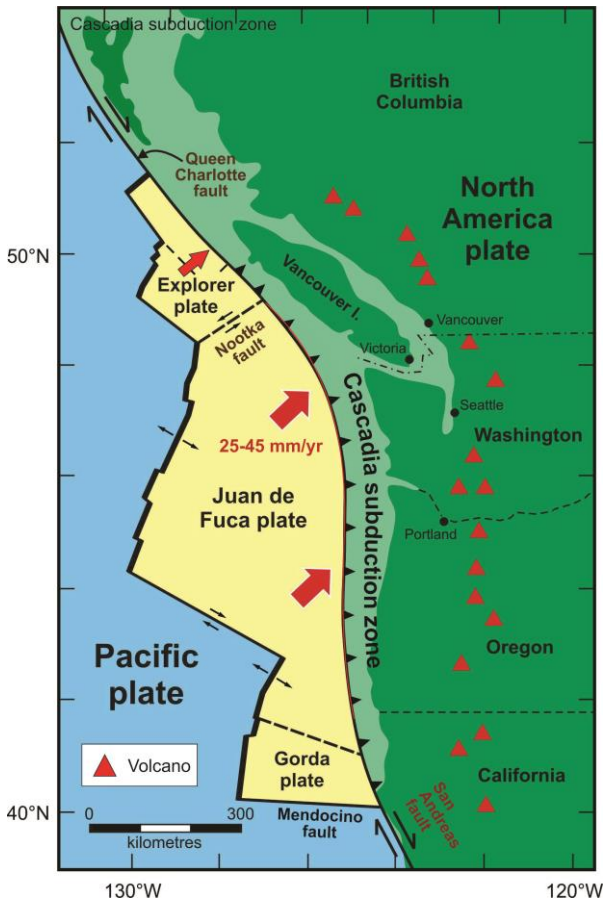

Figure 17. The Cascadia subduction zone, a convergent plate boundary stretching 1000 km from northern Vancouver Island (BC) to northern California. The Juan de Fuca Plate and two smaller plates are sliding beneath the North American Plate.

Cascadia Subduction Zone (CSZ) tsunamis are considered as the main tsunami threat for the west coast of British Columbia [*Clague et al.*, 2003; *Leonard et al.*, 2014]. Preliminary numerical modelling of CSZ tsunamis for coastal North America [cf. *Ng et al*., 1991; *Whitmore et al*., 1993; *Cherniawsky et al.*, 2007; *Fine et al.*, 2008; *Cheung et al*., 2011, *AECOM*, 2013] demonstrates the high threat of CSZ tsunamis for British Columbia. Numerous seismotectonic studies indicate that great megathrust earthquakes in the CSZ region have occurred on a regular basis in the past and can be expected to occur with an average return period of about 500 years in the foreseeable future [*Witter et al.*, 2013; *Wang and Tréhu*, 2016].

Based on recent advances in Cascadia tsunami source development [cf. *Wang and Tréhu*, 2016], *Fine et al.* [2018b] considered two different CSZ earthquake source models for tsunamis impacting the coast of British Columbia: Model A, the "buried" model; and Model B, the "splay" model. The models correspond to the same seismic momentum magnitude ($M_w = 9.0$) but to different cross-shore distributions of the associated seismic seafloor uplifts, h_0. The models have the northward extensions from the *Witter et al.* [2013] seismic sources off California to Washington, but also include source areas located to the west of Vancouver Island.

The splay-fault rupture ("Model M1") is of particular importance as it best represents a CSZ earthquake given present understanding of the faulting processes. For this model, *Witter et al.* [2013] used an extremely dense numerical mesh to allow accurate modelling of the surface-breaching rupture. The present work uses a slightly modified version of the model according to the recommendations of *Wang and Tréhu* [2016] to simulate the tsunami risk for Victoria. The splay-faulting rupture model includes a contribution from coseismic horizontal displacements to the initial tsunami wave field through a component of ocean surface uplift due to the horizontal motion of the steep ocean bottom slopes [*Gao*, 2016]. Numerical tsunami simulations reveal that including the deformation due to horizontal displacements in the source function results in an increase in the far-field tsunami amplitudes. The resulting coseismic vertical deformations (h_0) are shown in Figure 18.

Model A is the case when the source deformation slip is located well below the seabed, whereby the seafloor uplift has a smooth and gentle cross-shore profile, with maximum uplift of 4 m. Model B corresponds to the "splay" model, where the rapture edges are at the sea floor. This model is similar to the case "M1" in the *Witter et al.* [2013] classification and can be considered the most probable scenario. Maximum uplift is nearly 8 m. We note that the two previous models for Cascadia tsunami

sources for the BC coast, *Cherniawsky et al*. [2007] and *AECOM* [2013], used tsunami sources that are somewhere between Models A and B.

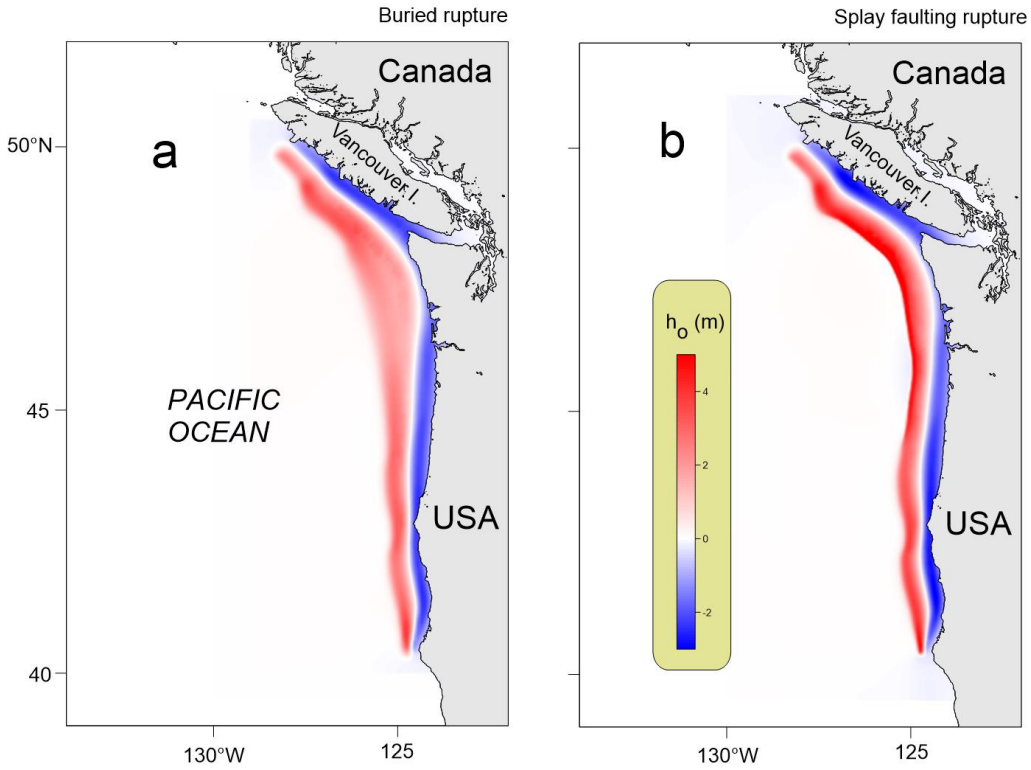

Figure 18. Maps of the Cascadia rupture zone tsunami sources according to *Gao* [2016]. Seafloor displacements, h_0, are in metres. (a) Whole margin buried rupture (Model A); and (b) Whole margin splay-faulting rupture (Model B). (From *Fine et al.* [2018b]).

Low-resolution results for CSZ tsunami simulations by *Fine et al.* [2018b] for Model A and Model B for Grid 1 (see Figure 7b) are presented in Figures 19a and 19b. As these models indicate, the tsunami amplitude maxima (wave crest maxima) for the open ocean are quite different: Model B provides much more intensive waves, with stronger interference of waves arriving from the northern and southern sectors of the CSZ. Waves generated by the splay faulting rupture (Model B) have a stronger impact on coastal areas of Vancouver Island and the US west coast than waves generated by the buried rupture (Model A).

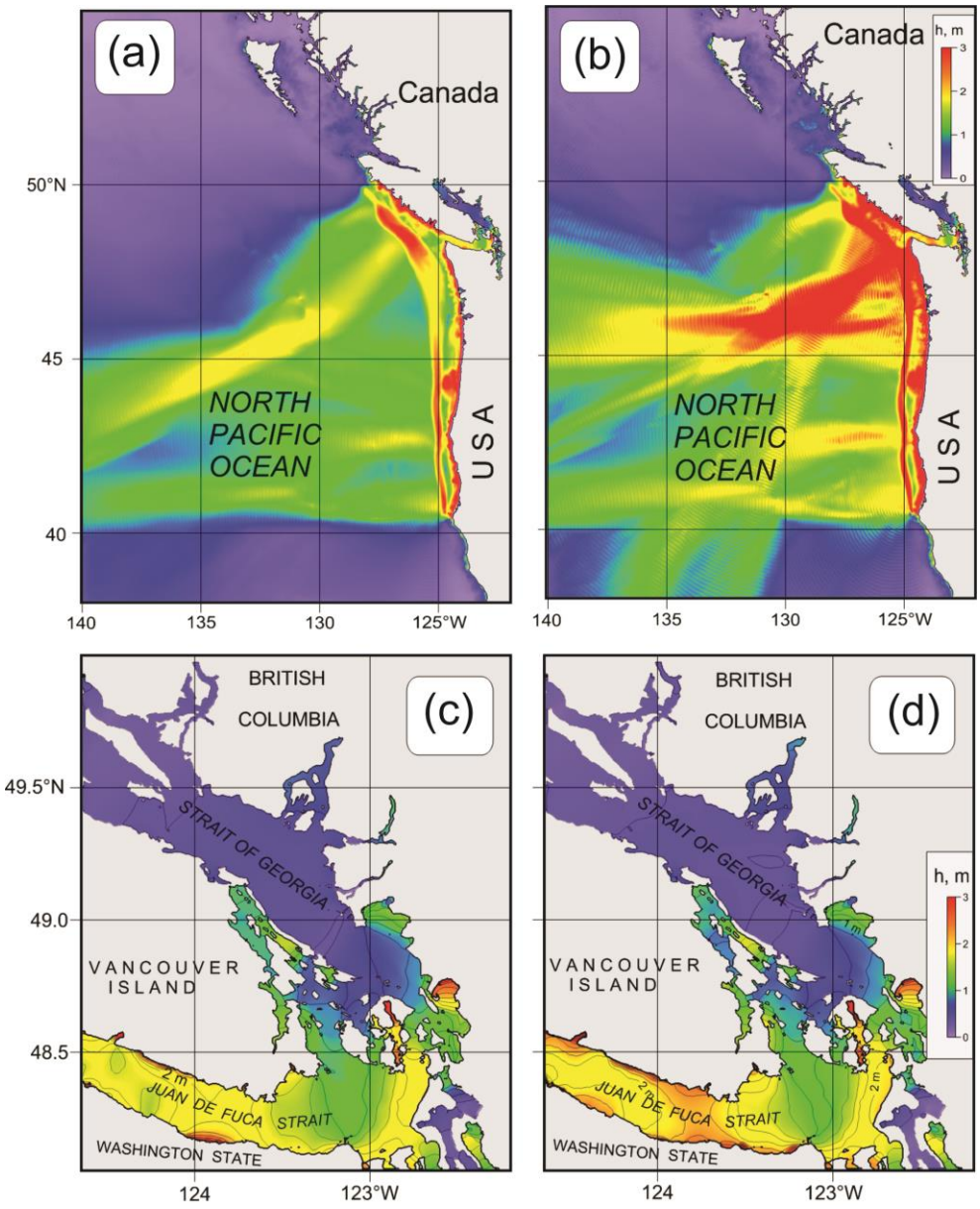

Figure 19. Spatial distribution of maximum tsunami wave amplitudes (*h*, in metres) for (a)-(b) Grid 1 and (c)–(d) Grid 2 of the nested-grid model for waves generated by simulation of the CSZ tsunami for (a)/(c) Model A; and (b)/(d) Model B. (Modified from *Fine et al.* [2018b]).

For southern Vancouver Island (Grid 2, Figures 19c and 19d), the differences between models A and B are less evident [*Fine et al.*, 2018b]. In general, Model B estimates higher wave amplitudes than Model A at the entrance and central part of Juan de Fuca Strait. At the eastern end of Juan de Fuca Strait and throughout the Strait of Georgia, the heights of the tsunami waves for Model A and

Model B are similar. However, around Victoria and Esquimalt harbours, model B simulates slightly larger tsunami waves.

Figure 20 shows the higher resolution Model A and B results for Grid 3, which covers the approach to Victoria and both Victoria and Esquimalt harbours. The resultant tsunami waves are approximately 15 to 20% higher for Model B than for Model A throughout entire Juan de Fuca Strait. The tsunami waves for both models are amplified slightly toward the southern (US) coast. The simulations also show amplification of the tsunami waves in these two harbours, especially in Esquimalt Harbour for both Model A and Model B.

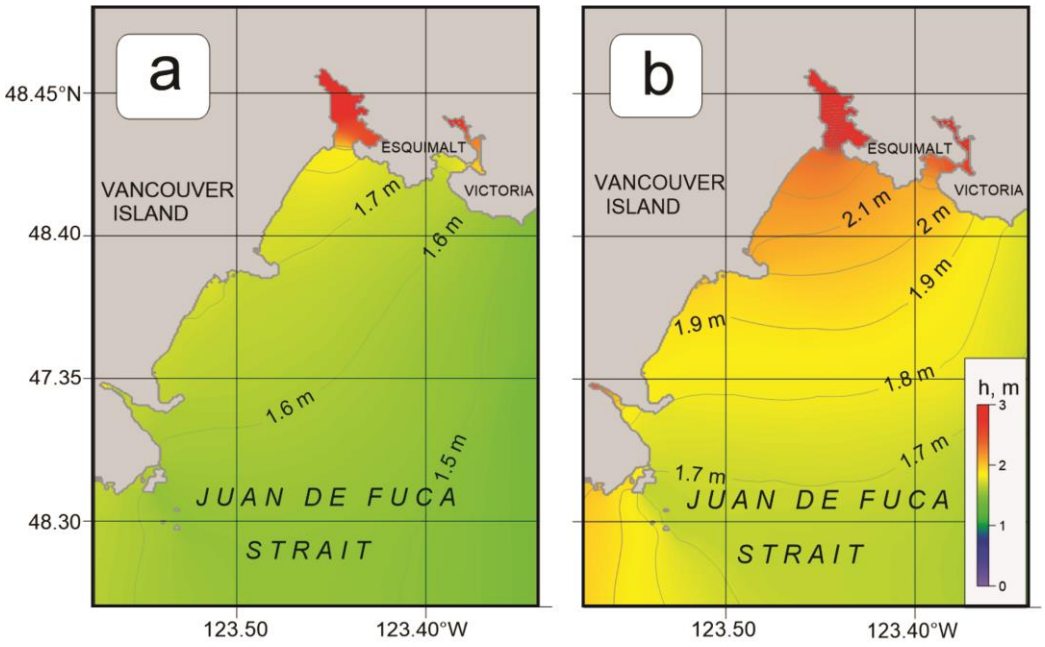

Figure 20. Spatial distribution of maximum tsunami wave amplitudes (*h*, in metres) for Grid 3 of the nested-grid model for waves generated by simulation of the CSZ tsunami for (a) Model A and (b) Model B. (Modified from *Fine et al.* [2018b]).

Detailed distributions of the maximum zero-to-crest wave amplitudes in Victoria Harbour and surrounding areas are presented in Figure 21. According to this figure, the spatial height distributions are quite similar for both models, but wave amplitudes for Model B are 30% higher than those for Model A: the mean maximum tsunami amplitudes are about 1.7 m and 2.2 m, respectively. Inside Victoria Harbour, tsunami amplitudes are nearly uniform and gently increase toward the harbour head and in the Gorge Waterway.

Time series for Models A and B for the simulated tsunami waveforms at specific sites are presented in Figures 22a and 22b; the statistical characteristics of these records are found in Tables 3 and 4. For each individual model run, the simulated wave amplitudes for Sites 2 to 7, located at the Canadian Coast Guard Base, are nearly identical, but differ notably from Sites 1 and 8. For both models, the wave heights are lower for Site 1 on the outer side of the water breaker and higher at Site 8, the tide gauge location.

Table 3. Tsunami wave parameters for a Cascadia Subduction Zone tsunami at Victoria for Model A numerical simulations. See Figures 21b and 21d for the site locations. Travel times for the maximum waves are in hours and minutes (hh:mm) after the start of the earthquake. (From *Fine et al.* [2018b]).

Site No	First trough		Highest crest		Deepest trough	
	Height (m)	Travel time hh:mm	Height (m)	Travel time hh:mm	Height (m)	Travel time hh:mm
1	-0.96	00:52	1.63	01:28	-1.04	02:58
2	-1.00	00:54	1.70	01:29	-1.16	02:56
3	-1.01	00:54	1.71	01:29	-1.16	02:56
4	-1.01	00:54	1.72	01:30	-1.17	02:56
5	-1.02	00:54	1.72	01:30	-1.19	02:57
6	-1.03	00:55	1.72	01:30	-1.22	02:57
7	-1.04	00:55	1.72	01:30	-1.22	02:57
8	-1.09	00:57	1.76	01:32	-1.33	03:00

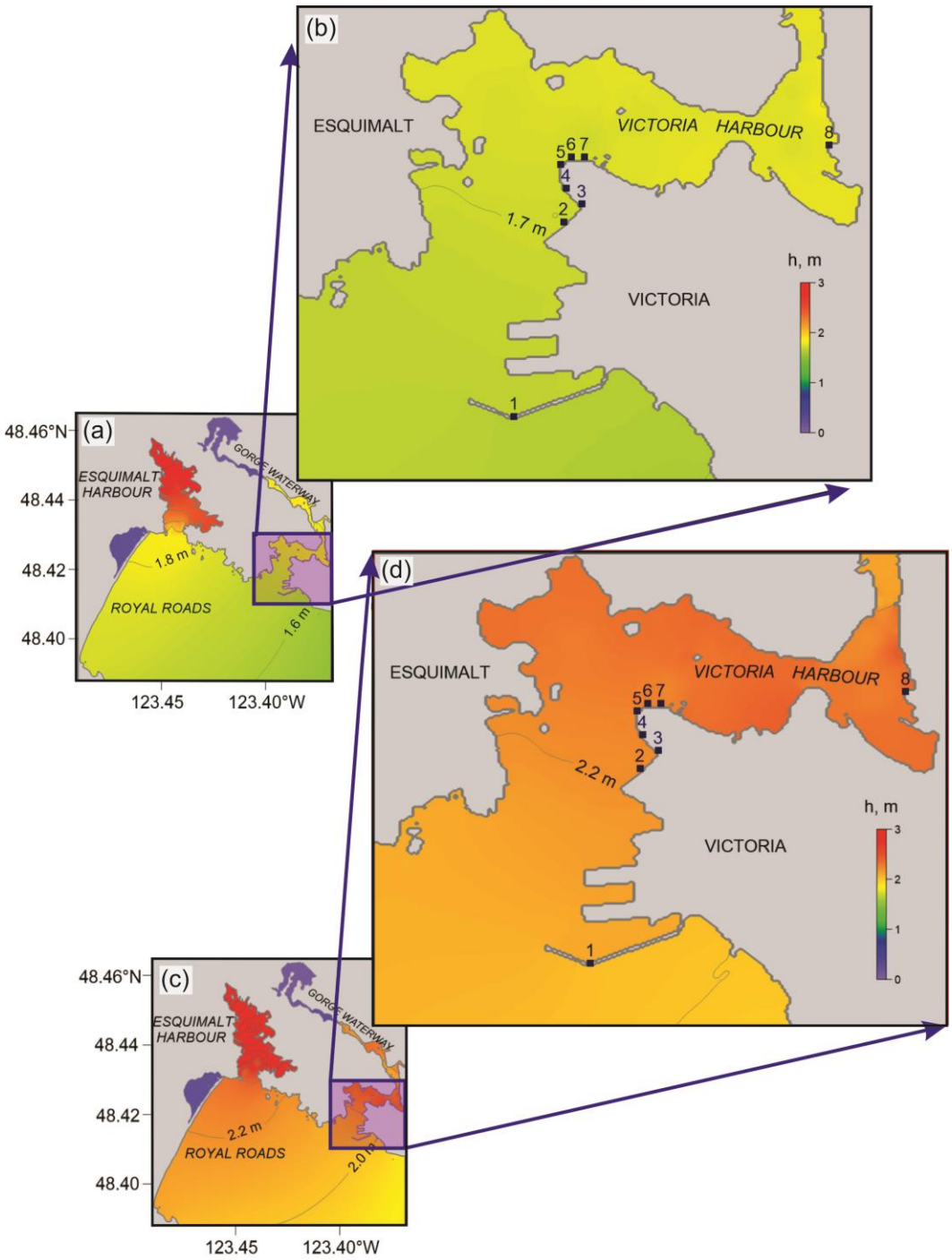

Figure 21. Spatial distribution of maximum tsunami wave heights (*h*, in metres) for (a)-(b) Grid 1 and (c)–(d) Grid 2 of the nested-grid model for waves generated by simulation of the CSZ tsunami for (a)/(c) Model A; and (b)/(d) Model B. Model A, Grid 4: Spatial distribution of maximum CSZ tsunami wave heights (*h*, m) for (a) Model A, Grid 4, (b) Model A, Victoria Harbour, (c) Model B, Grid 4 and (d) Model B, Victoria Harbour. (Modified from *Fine et al.* [2018b]).

Table 4. Tsunami wave parameters for a Cascadia Subduction Zone tsunami at Victoria for Model B numerical simulations. See Figures 21b, d for the site locations. Travel times for the maximum waves are in hours and minutes (hh:mm) after the start of the earthquake. (From *Fine et al.* [2018b]).

Site No	First trough		Highest crest		Deepest trough	
	Height (m)	Travel time hh:mm	Height (m)	Travel time hh:mm	Height (m)	Travel time hh:mm
1	-0.92	00:52	2.02	01:23	-1.24	03:01
2	-0.96	00:54	2.21	01:24	-1.38	03:03
3	-0.96	00:54	2.22	01:24	-1.38	03:03
4	-0.96	00:54	2.23	01:24	-1.38	03:03
5	-0.98	00:54	2.25	01:25	-1.38	03:03
6	-0.99	00:54	2.26	01:25	-1.38	03:04
7	-0.99	00:55	2.26	01:25	-1.23	03:04
8	-1.05	00:57	2.30	01:26	-1.49	03:08

According to *Fine et al.* [2018b], a CSZ-type earthquake will cause the land in the Victoria area to fall 20 cm immediately after the initial earthquake shock. As the leading wave of the incoming tsunami will be a wave trough, sea level in the region will also fall an additional 1 m upon arrival of the first wave roughly 54 min after the earthquake for both scenarios. After the initial drop caused by the leading wave, the sea level rises in the next half hour. At the Coast Guard locations (Sites 2 to 7), the highest wave crests reached are 1.72 m and 2.26 m at 1 hour 30 minutes and 1 hour 25 minutes after the earthquake for Models A and B, respectively.

The second wave crest is only slightly lower than the first crest wave for both cases; the third and subsequent waves are much lower than the first two waves. Typical tsunami wave periods are about 1 hour for both earthquake models. Tsunami waves generated by a mega-thrust earthquake along the CSZ will be quite strong in Victoria Harbour, reaching **1.7-2.3 m** in the vicinity of the Coast Guard Base. In addition to the high wave amplitudes (up to **2.26 m** for Model B), tsunamis will induce strong currents, up to **1.8 m/s** in the area adjacent to the Coast Guard Base [*Fine et al.*, 2018b].

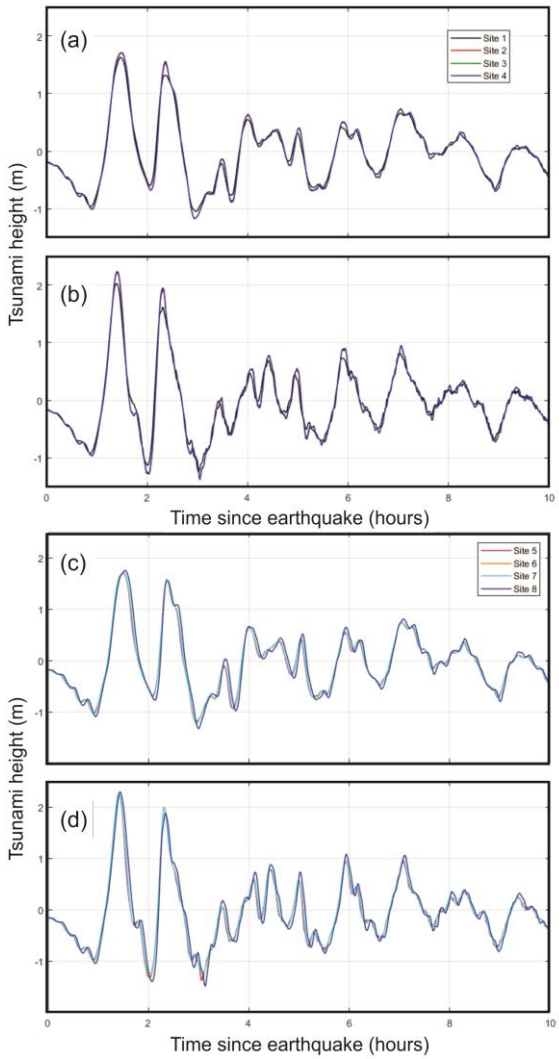

Figure 22. Simulated records of water level variations for a CSZ tsunami at Victoria Sites 1- 4 (a) Model A and (b) Model B and at Sites 5- 8 (c) Model A and (d) Model B. The site locations are shown in Figures 10b and 15c. (Modified from *Fine et al.* [2018b]).

Based on the modelling results, *Fine et al.* [2018b] provided the following summary and major conclusions:

- A high-resolution nested-grid tsunami model was used to simulate tsunami waves and wave-induced currents that will be generated in Victoria by a CSZ earthquake event. Two models of the earthquake rupture type and tsunami source region were used: Model A, a whole margin buried rupture; and Model B, a whole margin splay-faulting rupture. As recommended by international protocol, the numerical tsunami simulations were based on water depths for

Mean Higher High Water (MHHW) for the Victoria tide gauge site; MHHW is **0.73 m** above Mean Sea Level (MSL).

- The whole margin splay-faulting rupture scenario (Model B) generates higher waves in the Victoria area than the whole margin buried rupture scenario (Model A). Model B can be considered the "worst case scenario" for the area.
- The maximum wave amplitudes at the Coast Guard Base will be **1.72 m** (Model A case) and **2.26 m** (Model B case) above the tidal level at the time of the event; the first-crest wave will be the highest wave; the maximum tsunami wave heights will occur from 1h 25 min to 1 h 30 min after the start of the earthquake.
- Model B (the worst-case earthquake), together with the fact that a CSZ earthquake will cause the land in the Victoria region to suddenly subside by about 20 cm, will cause tsunami waves at the Victoria Coast Guard Base to reach a net maximum height of: 0.2 m +2.26 m + 0.73 m = **3.19 m** above MSL.
- Tsunami wave periods will range from 25 to 70 min.
- Tsunami wave amplitudes will be nearly spatially uniform throughout the Coast Guard Base location.
- Sea level will drop about **20 cm** immediately after the start of the earthquake due to land subsidence and the leading tsunami wave (a wave trough) will cause the water level to temporarily fall an additional 1 m below tidal level as it passes.

Because many of the details of future possible tsunamis remain unknown, including the tidal level at the time of the event, uncertainties in the earthquake source distribution, possible storm surge or other oceanic events, we recommend that a safety factor of 50 % be added, giving an estimated sea level height of **4.79 m** [=1.5×(2.26 m+0.73 m +0.2 m)] for a Model B-type CSZ tsunami.

4. GLOBAL AND REGIONAL SEA LEVEL RISE

The Intergovernmental Panel on Climate Change (IPCC) is a body of the United Nations that is dedicated to providing scientific information on climate change, its natural, political, and economic impacts and risks, and possible response options [*Weart,* 2011]. It was established in 1988 by the World Meteorological Organization (WMO) and the United Nations Environment Programme (UNEP) and endorsed by the UN General Assembly. The IPCC produces reports that contribute to

the work of the United Nations Framework Convention on Climate Change (UNFCCC), the main international treaty on climate change. The IPCC's Fifth Assessment Report was a critical scientific input into the UNFCCC's *Paris Agreement* in 2015.

In 2019, the IPCC published Special Report on the Ocean and Cryosphere in a Changing Climate (SROCC) with a specific Chapter 4 on sea level rise [*Oppenheimer and Glavovic*, 2019], while *James et al.* [2015, 2021] and *Lemmen et al.* [2016] prepared special reports considering sea level rise in West Canada, in particular, on the coast of British Columbia that take into account both global climatic sea level rise and vertical tectonic motions. *Rabinovich and Thomson* [2020] used these findings to evaluate the vertical sea level rise along the southeastern coast of Vancouver Island. The present chapter is based on this report, focussing on the Canadian Coast Guard Station in Victoria.

4.1. Climate change and global sea level rise

A Representative Concentration Pathway (RCP) is a greenhouse gas concentration trajectory adopted by the IPCC. Four main pathways were used for climate modeling and research for the IPCC fifth Assessment Report (AR5) in 2014. The pathways describe different climate futures, all of which are considered possible depending on the volume of greenhouse gases (GHG) emitted in the years to come. The RCPs – originally **RCP2.6**, **RCP4.5**, **RCP6**, and **RCP8.5** – are labelled after a possible range of radiative forcing values in the year 2100 (Figure 23) [*Moss*, 2008; *Weyant et al*., 2009].

The two most important RCPs are RCP4.5 and RCP8.5:

- **RCP 4.5** is described by the IPCC as an intermediate scenario (https://ar5-syr.ipcc.ch/topic_futurechanges.php). Emissions in RCP 4.5 peak around 2040-2050, then decline (Figure 23). Like all the other RCPs, RCP 4.5 requires negative CO_2 emissions (such as CO_2 absorption by trees) that would be 2 Gigatons of CO_2 per year (GtCO2/yr). RCP 4.5 is more likely than not to result in a global temperature rise of between 2°C and 3°C.

- In **RCP 8.5**, emissions continue to rise throughout the entire 21st century (Figure 23) [*Meinshausen et al.*, 2011]. RCP8.5 is generally taken as the basis for critical climate change *scenarios* since it is based on critical estimation of projected coal outputs. RCP8.5 remains useful for its aptness in both tracking historical total cumulative CO_2 emissions and predicting mid-century (and earlier) emissions based on current and stated policies.

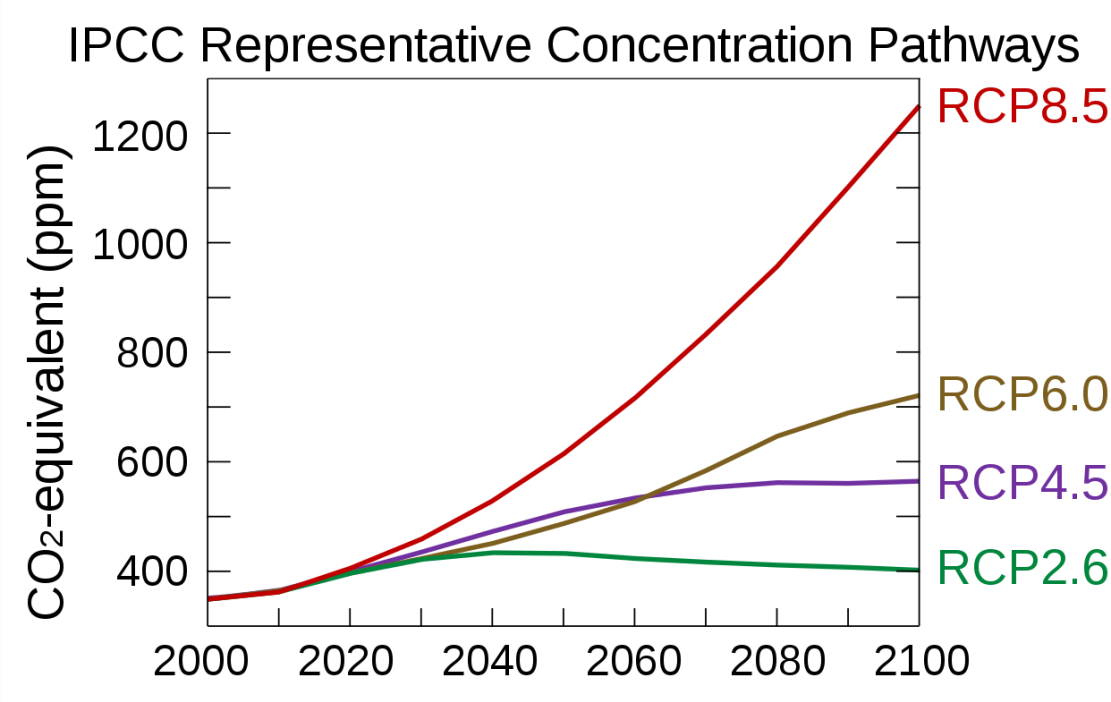

Figure 23. ICPC Representative Concentration Pathway (RCP) of CO_2-equivalent concentrations (in parts-per-million-by-volume) for 2000-2100. These four RCPs were used by the fifth IPCC Assessment Report to make predictions for sea level rise for the BC coast.

During the last 30 years, global mean sea levels (GMSL) rose by 3.66 mm per year which is 2.5 times faster than the rate from 1900 to 1990 (SROCC, 2019). At this rate of acceleration, sea level rise could reach around 30 cm to 60 cm by 2100 even if greenhouse gas emissions are sharply reduced and global warming is limited to well below 2°C, but around 60 cm to 110 cm if emissions continue to increase strongly. In their summary SROCC indicated that "*...rate of* ***rising sea levels is unprecedented*** *over the past century*".

Future sea level changes are of particular importance for planning infrastructure maintenance and development in the coastal zone, for habitat management and for forecasting risk to populations. Sea-level rise leads to increased frequency and strength of coastal flooding and is an important factor responsible for coastal erosion. One of the most serious consequences of sea-level rise is its effect on extreme sea levels, which are typically associated with tsunamis, storm surges, meteotsunamis and

other hazardous phenomena superposed on high tides. In the Pacific, large ENSO events can lead to significant sea-level changes (up to several tens of centimetres) [*Thomson et al.*, 2008].

Relative sea-level changes are observed or estimated relative to the solid surface of the Earth. Land uplift can offset global sea-level rise, leading to reduced rise or even fall of relative sea level; on the other hand, land subsidence adds to absolute sea-level rise and increases relative sea-level rise. Relative sea-level rise leads to increased coastal flooding and erosion, depending on the physical nature of the coastline, while relative sea-level fall can lead to navigation hazards owing to reduced depth-under-keel [cf. *James et al*., 2014, 2021; *Lemmen et al*., 2016; *Bush and Lemmen*, 2019].

The global sea-level rise projections presented in the IPCC Fifth Assessment Report are based on the Representative Concentration Pathways (RCP) scenarios (Table 5). The median projected sea-level rise of the highest emission RCP scenario (RCP8.5) is 1.7 times larger than that for the lowest emission RCP scenario RCP2.6 (Figure 24).

Table 5. Projections of changes in global mean temperature and sea level by 2100 under Representative Concentration Pathways scenarios (RCP) [*Rogelj et al.*, 2012].

RCP Scenario	Likely global surface temperature increase for 2081–2100* (°)	Likely global sea level rise for 2081–2100* (cm)
RCP2.6	0.3–1.7	26–55
RCP4.5	1.1–2.6	32–63
RCP6.0	1.4–3.1	33–63
RCP8.5	2.6–4.8	45–82

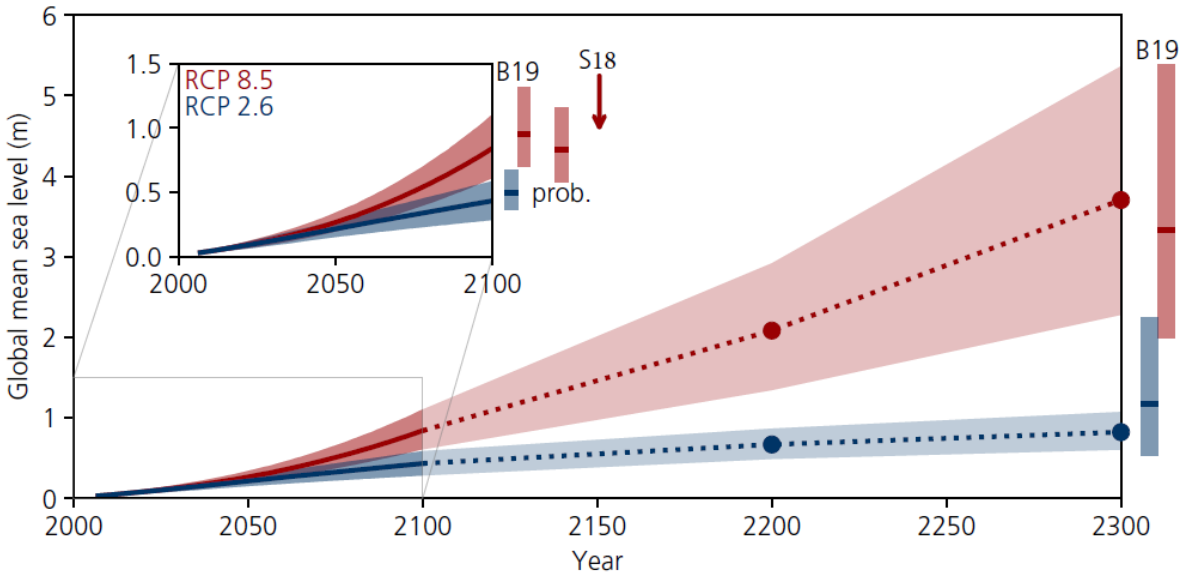

Figure 24. Projected sea-level rise until 2300. The inset shows an assessment of the likely range of the projections for RCP2.6 and RCP8.5 up to 2100 (*medium confidence*). Projections for longer time scales are highly uncertain but a range is provided. For context, results are shown from other estimation approaches in 2100. The two sets of two bars labelled B19 are from an expert elicitation for the Antarctic component and reflect the likely range for a 2 and 5° C temperature warming. The bar labelled "prob" indicates the likely range of a set of probabilistic projections. The arrow indicated by S18 shows the result of an extensive sensitivity experiment with a numerical model for the Antarctic ice sheet combined; as with the results for B19 and "prob. S18, the vertical bars show the *likely* range (from *Oppenheimer and Glavovic* [2019]).

Future rise in global mean sea level caused by thermal expansion, melting of glaciers and ice sheets, and land water storage changes, is strongly dependent on which RCP emission scenario is followed [*Oppenheimer and Glavovic*, 2019]. Sea level rise at the end of the century is projected to be faster under all scenarios, including those compatible with achieving the long-term temperature goal set out in the Paris Agreement. GMSL will rise between 0.43 m (0.29–0.59 m, likely range) for RCP2.6 and 0.84 m (0.61–1.10 m, likely range) for RCP8.5 by 2100 relative to 1986-2005 (Figure 24). Beyond 2100, sea level will continue to rise for centuries due to deep ocean heat uptake and mass loss of the Greenland and Antarctic ice sheets and with high confidence will remain elevated for thousands of years. Antarctica could contribute up to 28 cm of sea level rise (RCP8.5, upper end of likely range) by the end of the century (medium confidence) [*Oppenheimer and Glavovic*, 2019].

Under RCP8.5, the rate of sea level rise will be 15 mm/yr in 2100, and could exceed several cm/yr in the 22nd century. These high rates challenge the implementation of adaptation measures that involve a long lead-time but has not yet been studied in detail. *James et al.* [2014, 2021] and *Lemmen et al.* [2016] emphasize that the possibility of global sea-level rise exceeding 1 m by 2100 cannot be rejected and should be taken into account for estimation of possible extreme sea levels for the coast of British Columbia.

4.2. Sea Level rise for the British Columbia Coast

As indicated by *Oppenheimer and Glavovic* [2019], sea level does not and will not rise uniformly. Thermal expansion, ocean dynamics and land ice loss contributions will generate regional departures of about ±30% around the GMSL rise. Local anthropogenically-induced subsidence and change in wave height and period are important contributors to future changes in relative sea level (RSL) at the coast. Subsidence caused by human activities is currently the most important cause of RSL change in many delta regions. An important additional factor strongly influencing long-term sea level variations in specific regions are vertical land motions [*Lemmen et al.*, 2016]. They strongly influence changes in relative sea level. Land uplift will reduce the amount of sea-level rise experienced at a site; conversely, land subsidence will add to the amount of relative sea-level rise. Present-day land uplift or subsidence is measured using Global Positioning System (GPS) technology and by Global Navigation Satellite Systems. This factor is especially important for seismically active zones such as the coast of British Columbia. Local processes are critical for projections of sea level impacts at local scales. Due to projected global mean sea level rise, extreme sea level events (ESLs), including those related to tsunamis and powerful storm surges, that are historically rare may become common by 2100 under all RCPs.

A dominant factor affecting relative sea-level change in British Columbia (as well as the rest of Canada) is vertical land motion. Vertical land movements in British Columbia arise from a combination of tectonic activity due to the interactions of the Juan de Fuca and Pacific oceanic plates with the North America plate, the land moving upward in response to the weight removed when the glaciers of the last ice age melted (glacial isostatic adjustment) and present-day ice-mass changes in the Coast Mountains and the Gulf of Alaska. On the Fraser River delta, sediment compaction contributes to land subsidence [*Thomson et al.*, 2008; *Bornhold and Thomson*, 2013]. Global

Positioning System (GPS) observations show that the land is rising faster on the west coast of Vancouver Island than at Victoria and Vancouver, explaining why sea level has been falling at Tofino during the last 50 years but rising at Victoria and Vancouver.

Lemmen et al. [2016] in Chapter 7 of their report describe in detail the situation for the west coast of Canada. The authors emphasized that coastal British Columbia is geographically, ecologically and socially diverse. The climate changes anticipated for this region, and their impacts, are similarly varied. Nevertheless, several key findings are relevant to the region as a whole:

- Sea-level rise will not affect all areas of the British Columbia coast equally, largely due to differences in vertical land movement.
- The largest relative sea-level rise is projected to occur on the Fraser Lowland, southern Vancouver Island and the north coast.
- Storm-surge flooding presents a greater threat to coastal communities than sea-level rise alone. Extreme water levels can be associated with climate variability (e.g., El Niño/La Niña Southern Oscillation) and storm-surge flooding. The risks associated with these events are expected to increase as sea level rises.
- Planning guidance for sea-level rise developed by the British Columbia government provides planning levels that slightly exceed the peak values (95%) of the sea-level projections at 2050. This could be considered a margin of safety that allows for possible additional sea-level rise arising from factors with significant uncertainty, such as contributions from the Antarctic Ice Sheet.

Using all previous findings, *James et al.* [2021], prepared maps of relative sea level changes on the coasts of British Columbia at 2050 and 2100 for the worst case (high-emissions) scenario, RCP8.5 (Figure 25) and moderate (median) scenario, RCP4.5 (Figure 26).

According to the mapping results, the high-end predicted rise in relative sea level for the area of Nanaimo and Patricia Bay is 20-30 cm for 2050 (Figure 3a), increasing to 80-100 cm for Patricia Bay and 60-80 cm for Nanaimo for 2100 (Figure 3b). Similar *median estimates* (RCP4.5) for 2050 are 15-20 cm (Patricia Bay) and 10-15 cm (Nanaimo) (Figure 4a) and for 2100 are 40-60 cm (Patricia Bay) and 20-40 cm (Nanaimo) (Figure 4b).

Long-term Canadian Hydrographic Service (CHS) tide gauge measurements were used by *James et al.* [2015] to predict sea level rise at specific sites in British Columbia, taking into account both global sea level rise associated with climatic changes and vertical land motions. The

corresponding estimates for Victoria are presented in Figure 27. The relative projected sea level changes for various RCP values and years for this station are shown in Table 6. For comparison, similar estimates for Patricia Bay and Campbell River are also included into this table.

Hausfather and Peters [2020] indicate that, fortunately, the world imagined in RCP8.5 is one that, in their view, becomes increasingly implausible with every passing year. As the authors of this papers state: *"We must all — from physical scientists and climate-impact modellers to communicators and policymakers — stop presenting the worst-case scenario as the most likely one.* ***Overstating the likelihood of extreme climate impacts can make mitigation seem harder than it actually is.*** *This could lead to defeatism, because the problem is perceived as being out of control and unsolvable. Pressingly, it might result in poor planning, whereas a more realistic range of baseline scenarios will strengthen the assessment of climate risk.* ***Stop using the worst-case scenario for climate warming as the most likely outcome — more-realistic baselines make for better policy.****"*

At the same time, as *James et al.* [2021] indicated, for comparative analyses of the costs of mitigation and adaptation, comparisons between a *high-emissions scenario* (RCP8.5) and *a low-emission scenario* (RCP2.6, strong mitigation), may be useful. Here the impacts and costs of climate change for differing pathways of carbon emissions can be assessed and compared to the costs of mitigation.

Taking into account the recommendations of *Hausfather and Peters* [2020] and *James et al.* [2021], we selected from the tables and results presented in Figures 25-27 of *James et al.* [2015, 2021] the *median values* of projected relative sea-level changes at Victoria. The sea-level projections are based on a national model of vertical crustal motion derived from GPS measurements [*Robin et al*., 2020]. An important fact follows from these results: a significant tectonic subsidence of the west coast of Vancouver Island in the central part of the island. For this region the indicated subsidence significantly compensates the general Global Sea Level Rise. However, in the area of Victoria this effect is not significant (Figure 28); therefore, the expected sea level changes for the period 2050-2200 are mostly determined by the climatic sea level changes.

As indicated by Table 6, the relative projected sea level changes at Victoria and Patricia Bay are very similar: approximately 35 cm for RCP2.6 and 54 cm for RCP8.5 (for 2100). For comparison, the corresponding values for Campbell River are much smaller [*Rabinovich and Thomson,* 2020]: 10 and 28 cm, respectively. This is just because the negative vertical tectonic motions in the area of Campbell River compensate the positive climatic sea level changes. Comparative results for four BC

stations are shown in Figure 28. From this figure it is clear that the tectonic subsidence at Campbell River is 3.5 mm/year, at Ucluelet 2.5 mm/year, but at Victoria only 0.5 mm/year.

In our study we used some very recent results presented to the authors by *Thomas James* (National Resources, Canada). The corresponding plots are shown in Figure 29. They enable us to estimate the general spatial structure of projected relative sea-level changes in Juan de Fuca Strait and in the Strait of Georgia and, in particular, for the Victoria region. They also give us some extrapolated values for 2200.

All final results of projected sea level changes at Victoria for 2050, 2100 and 2200 are presented in Table 7. These values were used to evaluate possible coastal flooding due to various marine sea level hazards for the area of Victoria under *low, moderate and high* global sea level rise scenarios. For comparison, based on results of *Rabinovich and Thomson* [2020], we have also included similar estimates for Patricia Bay (IOS) and Departure Bay, Nanaimo (PBS).

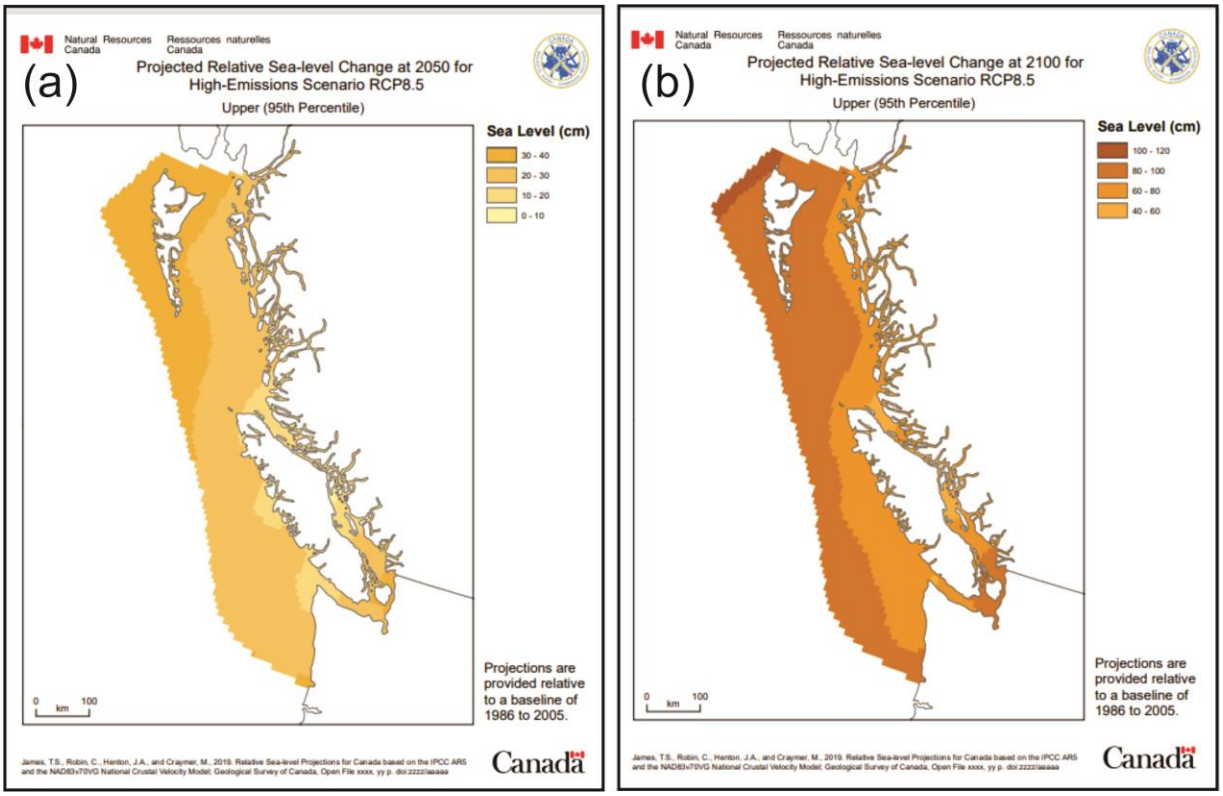

Figure 25. Projected relative sea-level changes at (a) 2050 and (b) 2100 for high-emissions scenario RCP8.5. Upper (95%). (From *James et al.* [2021]).

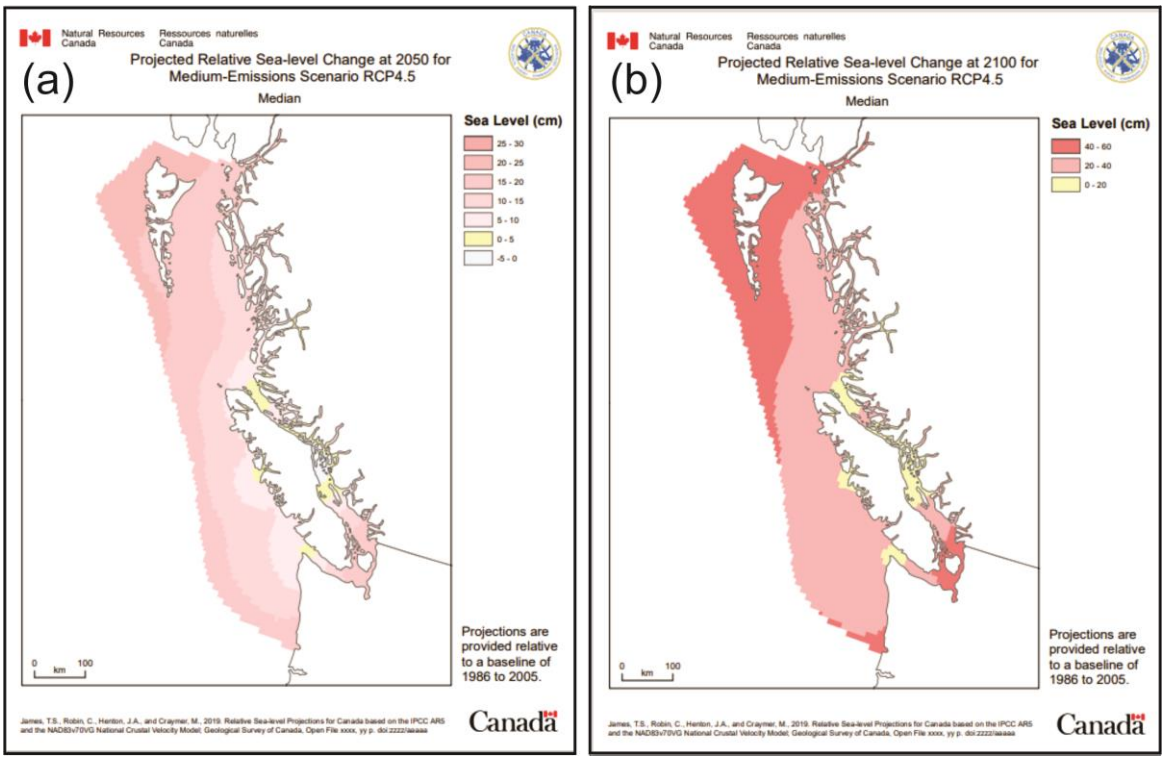

Figure 26. Projected relative sea-level changes at (a) 2050 and (b) 2100 for medium-emissions scenario RCP4.5. Median. (From *James et al.* [2021]).

Table 6. Relative projected sea level changes (median values) for Victoria, Patricia Bay and Campbell River (in cm) for 2050 and 2100 based on estimates by *James et al.* [2015] (for Victoria see Figure 25; Patricia Bay and Campbell River are shown in Figures 5 and 6 of *Rabinovich and Thomson* [2020]).

RCP	Victoria		Patricia Bay		Campbell River	
	2050	2100	2050	2100	2050	2100
2.6	15.0	36.1	13.9	34.0	1.2	10.1
4.5	15.5	40.1	14.3	38.0	1.9	14.0
8.5	16.1	54.6	15.0	52.4	2.4	28.3

Victoria, BC (ALBH)

Projected sea-level change is given in centimetres, relative to 1995.

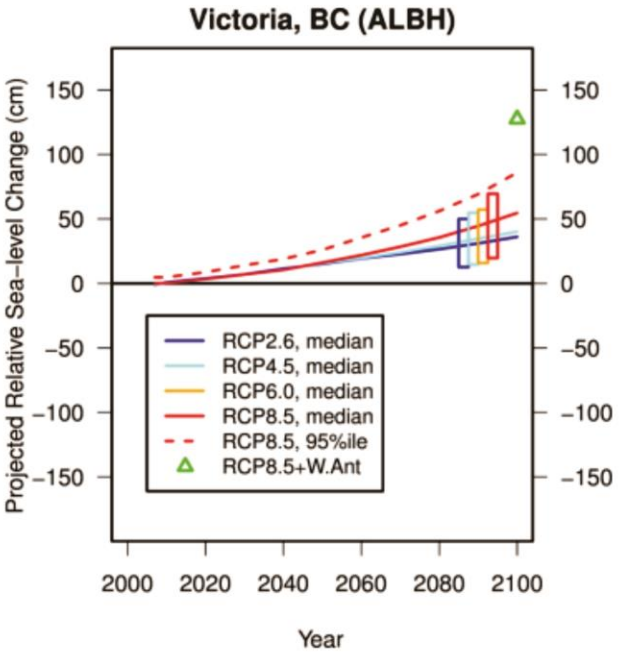

Figure 37. Projected relative sea-level change for RCP2.6, RCP4.6, and RCP8.5 (median values, solid lines; 95th percentile of RCP8.5, dashed line) (James et al., 2014). Rectangles also include RCP6.0 and give the 90% confidence range (5% to 95%) of the average for the time period 2081-2100. RCP8.5 +W.Ant is the median projection of RCP8.5 plus an additional 65 cm of global sea-level rise from West Antarctica(green triangle).

Average Projected Sea-level Change, 2081-2100

scenario	5%	median	95%
RCP2.6	12.6	31.3	50.0
RCP4.5	14.6	34.7	54.8
RCP6.0	15.8	36.5	57.2
RCP8.5	19.7	44.6	69.5

RCP8.5+W.Ant at 2100: 127.3 cm

RCP2.6

year	5%	median	95%
2007	-3.9	-1.1	1.7
2010	-3.8	0.8	5.4
2020	-1.1	3.8	8.6
2030	0.9	7.0	13.1
2040	2.6	11.4	20.3
2050	6.0	15.0	24.0
2060	7.5	19.2	30.9
2070	9.7	22.7	35.7
2080	10.3	26.5	42.7
2090	11.6	31.0	50.4
2100	13.7	36.1	58.6

RCP4.5

year	5%	median	95%
2007	-4.1	-0.8	2.5
2010	-3.9	0.3	4.4
2020	-1.5	3.1	7.8
2030	0.0	6.7	13.3
2040	2.2	10.5	18.8
2050	6.9	15.5	24.0
2060	7.4	19.5	31.5
2070	9.9	23.9	38.0
2080	11.8	29.0	46.2
2090	14.7	34.7	54.7
2100	16.6	40.1	63.7

RCP8.5

year	5%	median	95%
2007	-4.9	-0.1	4.7
2010	-4.5	0.2	4.8
2020	-1.8	3.4	8.7
2030	-0.2	6.9	14.0
2040	2.2	10.5	18.9
2050	6.3	16.1	26.0
2060	8.2	21.9	35.5
2070	11.8	28.4	45.0
2080	15.1	35.6	56.1
2090	19.7	44.5	69.2
2100	23.3	54.6	85.9

Figure 27. Projected relative sea-level changes at Patricia Bay for 2007-2100 for RCPs 2.6, 4.5 and 8.5 (From *James et al.* [2015])

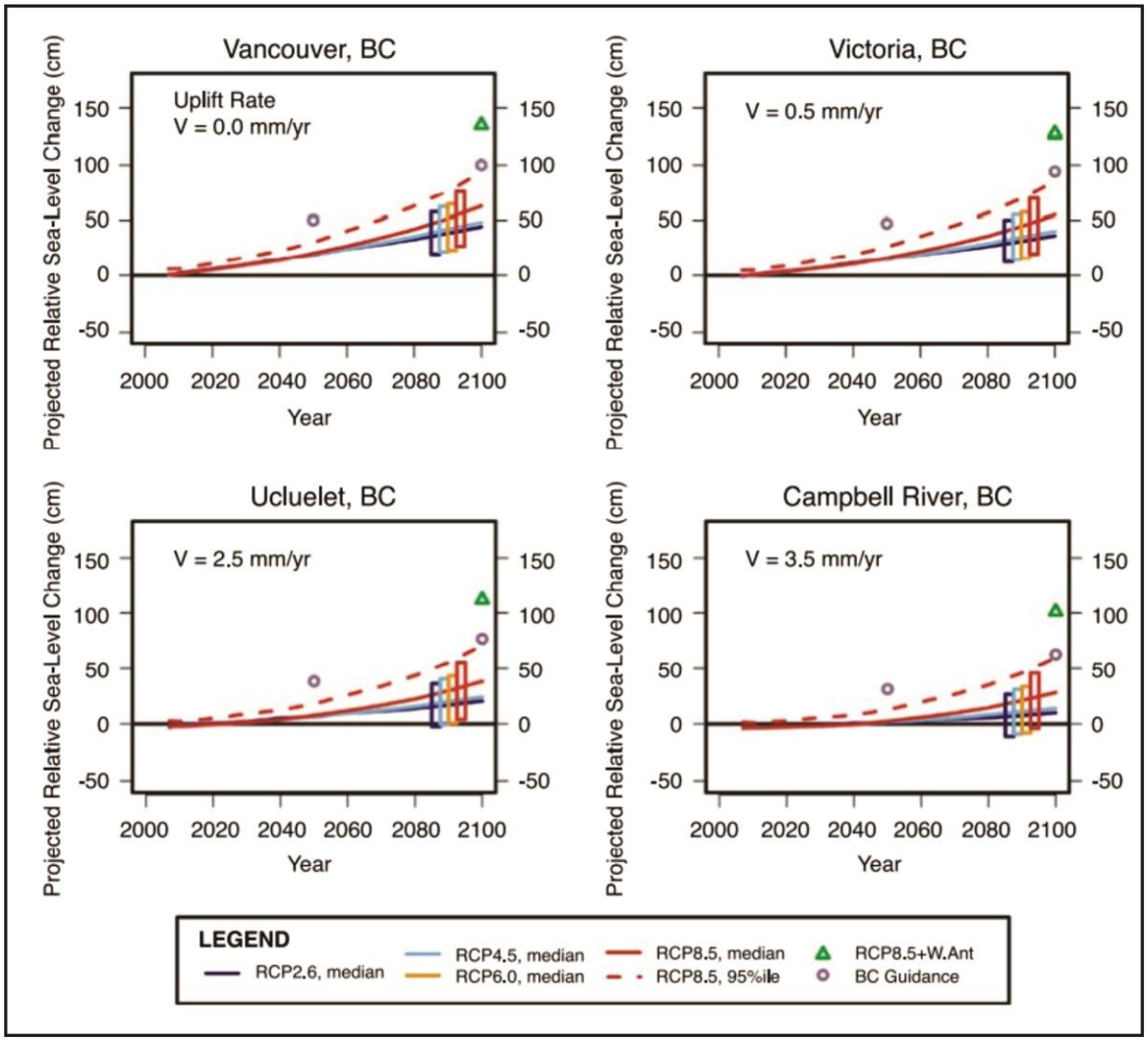

Figure 28. Projected relative sea-level change through the 21st century for selected communities in British Columbia (after *James et al.* [2015]). RCP2.6 is a low-emissions scenario, RCP6.0 is an intermediate-emissions scenario and RCP8.5 is a high–emissions scenario. The projected value for 2100 is also given for the high-emissions plus Antarctic ice-sheet reduction scenario, an augmented scenario in which West Antarctica contributes an additional 65 cm to the median projected value of the high-emissions scenario (RCP8.5+W.Ant; green triangle). Rectangles show the 90% confidence interval (5–95%) of the average projection for the period 2081-2100 and include RCP6.0. The dashed red line gives the 95th percentile value for the high-emissions scenario. Vertical land motion is given to the nearest 0.5 mm/year in each panel. (From *Vadeboncoeur* [2016])

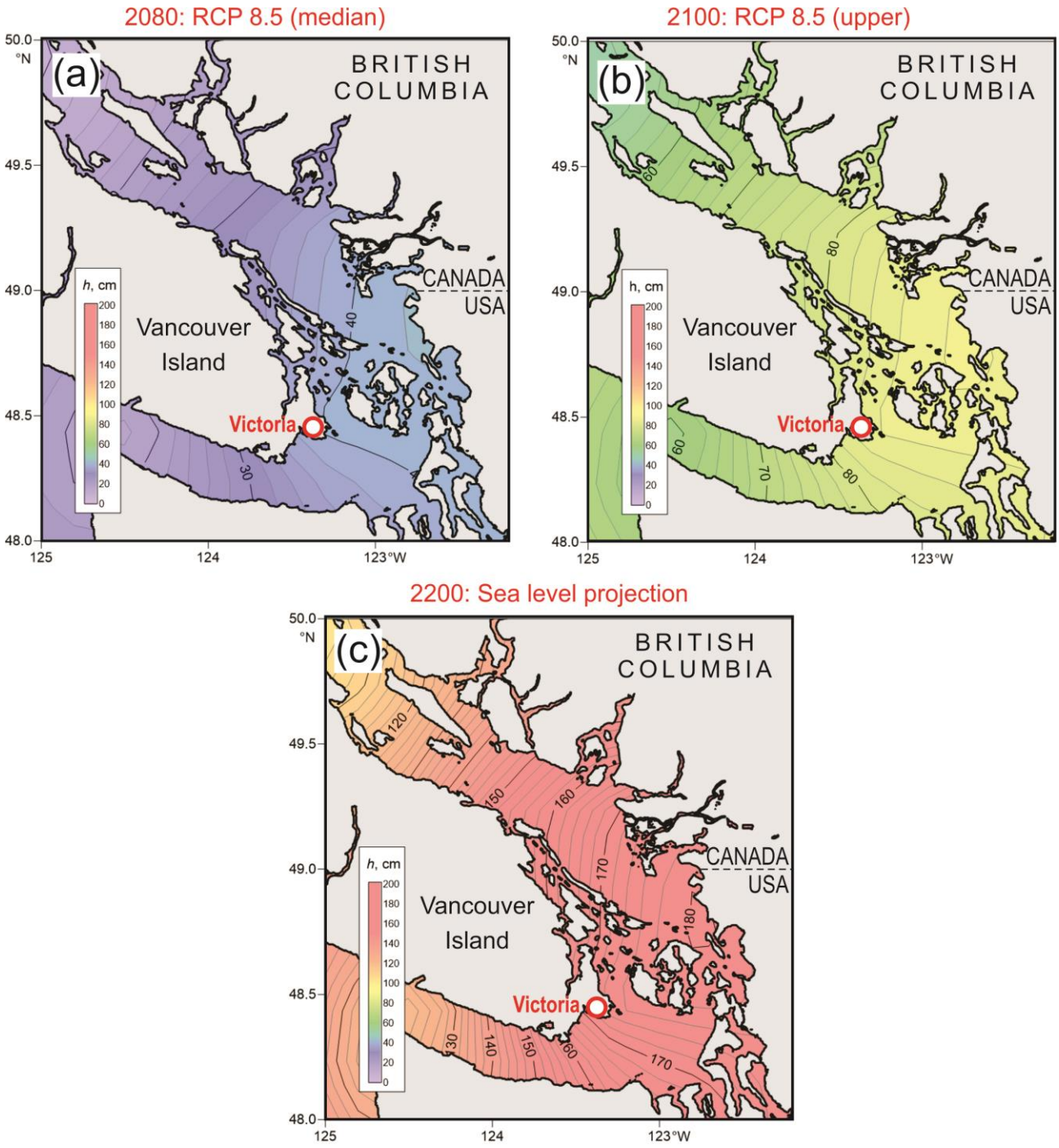

Figure 29. Projected relative sea-level changes for Juan de Fuca Strait and the southern Strait of Georgia for (a) 2080, scenario RCP8.5 (median), (b) 2100, RCP8.5 (upper) and (c) 2200 sea level projection (Constructed by Isaac Fine based on data provided by Thomas James, National Resources of Canada [*James et al.*, 2021]).

Table 7. Relative projected sea level changes (median values) for Victoria, Patricia Bay and Nanaimo (in cm) for 2050, 2100 and 2200.

Year	Victoria		Patricia Bay		Nanaimo	
	RCP4.5	RCP8.5	RCP4.5	RCP8.5	RCP4.5	RCP8.5
2050	15	16	14	15	8	9
2100	40	55	38	52	26	40
2200	~125	175	?	166	?	154

5. EFFECT OF SEA LEVEL RISE ON TSUNAMI HEIGHTS

In this section we can combine the results of Sections 3 and 4 to estimate the tsunami risk for the Victoria area and, in particular, for the Victoria Coast Guard Station taking into account the expected long-term sea level changes caused by the global climatic sea level rise and vertical tectonic motions. The main results of this combination are shown in Figure 30. The maximum tsunami amplitudes in this figure were computed for (a) a 1964-type Alaska tsunami, and (b) for a 1700-type CSZ (Model B) tsunami. The **20-cm** land subsidence expected for the CSZ earthquake is also included. The total tsunami heights are shown in this figure relative to mean sea level (MSL) and relative to mean higher-high water, MHHW = 73 cm for Victoria. All estimates are for 2100 for the three Representative Concentration Pathway (RCP) Scenarios: *Low* (RCP2.6), *moderate* (RCP4.5) and *high* (RCP8.5).

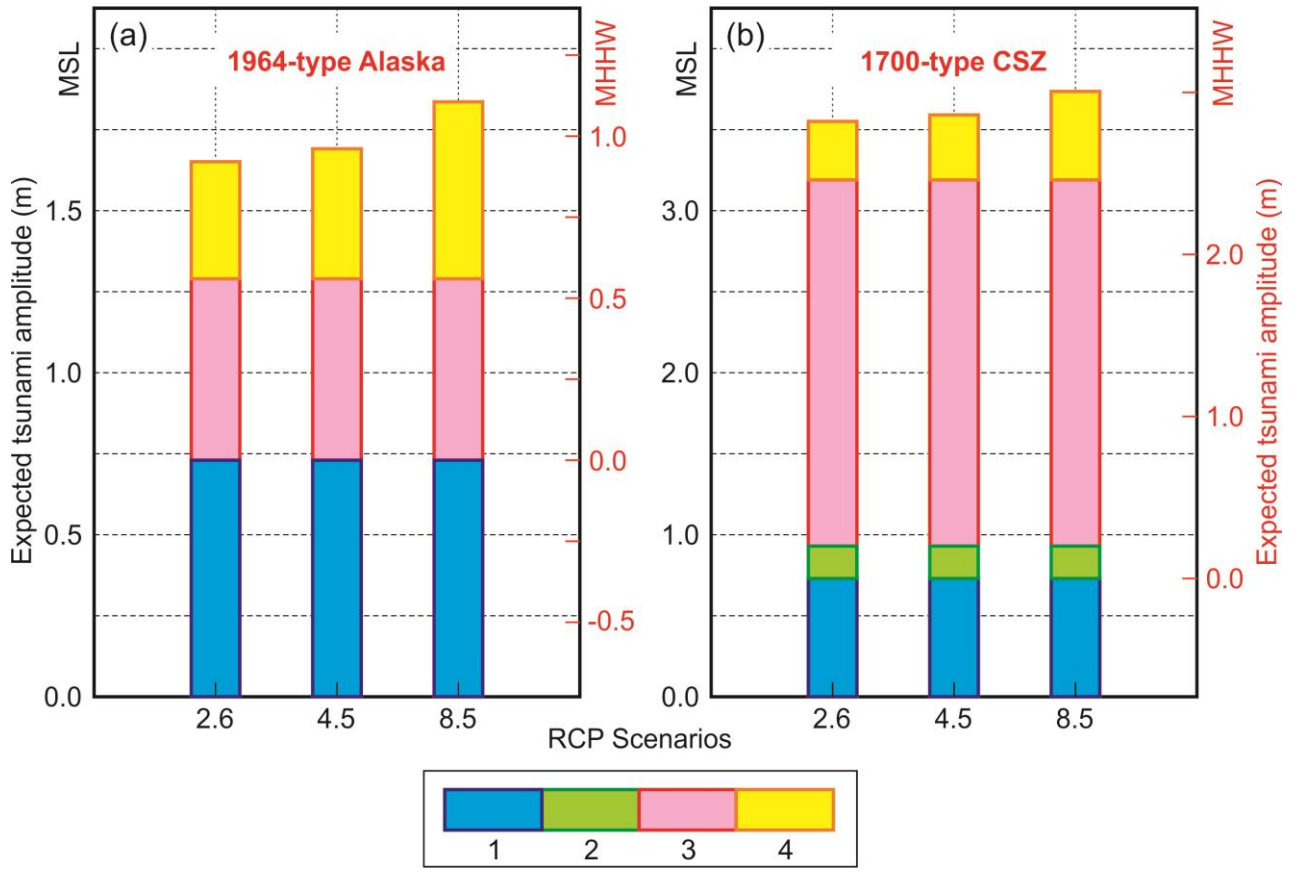

Figure 30. Expected effective tsunami heights numerically simulated by *Fine et al.* [2018a,b] for (a) a 1964-type Alaska and (b) a 1700-type CSZ (Model B) earthquake, taking into account possible sea level change for 2100 produced by the combined effect of global sea-level rise for Representative Concentration Pathway (RCP) Scenarios RCP2.6 (*low*), RCP4.5 (*moderate*) and RCP8.5 (*high*). Along the left Y-axis are the expected tsunami wave amplitudes relative to mean sea level (MSL); along the right Y-axis tsunami wave amplitudes are relative to mean higher-high water (MHHW = 73 cm for Victoria). In the colour-coded legend: "1" is the MHHW level; "2" is the land subsidence accompanying a CSZ-type tsunami; "3" is the computed tsunami wave amplitude; and "4" is the expected sea level rise.

In summary, all components of the forecasted sea levels (in cm) for the two types of earthquakes can be presented as follows:

	Alaska	CSZ
MHHW	73	73
Land subsidence	0	20
Tsunami amplitude	56	226
RCP2.6	36	36
RCP4.5	40	40
RCP8.5	55	55
Total (RCP2.6)	**165**	**355**
Total (RCP4.5)	**169**	**359**
Total (RCP8.5)	**184**	**374**

Because many of the details of future possible tsunamis remain unknown , including the tidal and seasonal sea levels at the time of the event, uncertainties in the earthquake source distribution, possible storm surge or other oceanic events, we recommend that a safety factor of 50% be added, giving an estimated tsunami-generated sea level height: of **1.94 m** (=1.5×(0.56 m+0.73 m) for a 1964-type Alaska tsunami and **4.79 m** (=1.5×(2.26 m+0.73 m +0.2 m)) for a Model B-type CSZ tsunami. The total effective wave heights in that case will be:

	Alaska	CSZ
Total (RCP2.6)	**2.30 m**	**5.15 m**
Total (RCP4.5)	**2.34 m**	**5.19 m**
Total (RCP8.5)	**2.49 m**	**5.34 m**

All predictions are for the year 2100; for 2200 we need to add ~**0.85 m** for RCP4.5 and **1.2 m** for RCP8.5.

6. DISCUSSION AND CONCLUSIONS

Large segments of the British Columbia coast are susceptible to floods produced by trans-oceanic tsunamis. An additional problem for this area, as well as other coastal regions of British Columbia, are Global Sea Level Rise and vertical tectonic land motions. The main focus of the present study was the tsunami risk to the Victoria Coast Guard Station under projected sea level rise conditions. The study begins with an examination of the general historical information on tsunamis observed within Victoria Harbour, the results of numerical modelling by *Fine et al.* [2018a,b] of two potentially most dangerous seismically generated tsunamis (a 1964-type Alaska and a 1700-type Cascadia Subduction Zone tsunami), and their risk for the study region, specified by taking into account the vertical motion of Vancouver Island and climatic-induced sea level rise.

Victoria has one of the world-longest tsunami measurement periods: from 1910 to 2021. During this period, 39 tsunamis were recorded at Victoria, including 22 during 2000-2020, when precise digital sea level observations began to be provided for the British Columbia coast. Examination of the recorded wave statistics indicates that only seven major events at Victoria exceeded the 20-cm threshold tsunami wave height level (i.e., when tsunami wave amplitudes were >10 cm). The earthquake source events for the tsunamis are: 1946 Aleutian Islands (M_w 8.6); 1952 Kamchatka (M_w 9.0); 1957 Aleutian Islands (M_w 8.6); 1960 Chile (M_w 9.5); 1964 Alaska (M_w 9.2); 2010 Chile (M_w 8.8); and 2011 Tohoku (M_w 9.1). During the 1910-2021 period, the Tofino tide gauge (the "beacon station" for the Canadian Tsunami monitoring system) recorded 70 tsunamis, including all 39 events that were detected at Victoria. At Tofino, the seven major tsunamis detected at Victoria exceeded the 40-cm threshold wave height.

Parameters of the seven major tsunamis recorded at Tofino and Victoria enabled us to estimate empirical relationships between the observed maximum tsunami wave eights, H, and arrival times between these two stations. Specifically, $H_{Vict}/H_{Tof} \approx \mathbf{0.57\pm0.03}$, while the lead time differences for Tofino relative to Victoria were from 69 min (for Aleutian-Alaska tsunamis) to 34 min (for Chilean tsunamis). These estimates show that Tofino can be effectively used to forecast tsunami waves at Victoria.

Of the seven major recorded events, only the 1964 event generated tsunami waves that were hazardous to Victoria Harbour and, in particular, to the CCG site. The 1964 Alaska "Good Friday" tsunami destructively affected the twin cities of Alberni and Port Alberni and created significant damage in and around Prince Rupert. At Victoria, the first wave had a height h_{tsu} = 147 cm. It should

be noted that any tsunami of wave height h_{tsu} > 100 cm (1 m) is considered to be potentially destructive, in particular because of the strong currents associated with the waves. It is evident that great Alaska earthquakes, with M_w = 9.0-9.3, can be a major threat to the Victoria area.

Another, and even more important tsunami threat for the coast of British Columbia, are Cascadia Subduction Zone (CSZ) earthquakes [cf. *Leonard et al.*, 2014]. The Great CSZ earthquake of 26 January 1700, which had an estimated magnitude M_w = 9.0, generated a major trans-oceanic tsunami that, according to paleotsunami studies, strongly affected the outer coast of British Columbia [cf. *Clague et al.*, 2000, 2003].

These two types of tsunami, the 1964-type Alaska and the 1700-type CSZ, were numerically simulated by *Fine et al.* [2018a,b] to estimate the tsunami risk for the vicinity of the Victoria Coast Guard Station. Their model was based on a finite-difference nested-grid formulation of the linear shallow-water equations and is similar to well-known tsunami models, TUNAMI and COMCOT [*Imamura*, 1996; *Liu et al.*, 1998; *Imamura et al.*, 2006]. For both the 1964 Alaska and 1700 CSZ events, *Fine et al*. [2018a, b] used a series of four nested grids; Grid 3 and Grid 4 were the same for both projects, while Grid 1A and 2A for the 1964 Alaska project were different from Grid 1B and 2B for the 1700 CSZ project. These grids made it possible to achieve high spatial resolution and to accurately resolve the reflection and transformation of the tsunami waves on the shelf of Vancouver Island, in Juan de Fuca Strait and in Victoria Harbour.

The modelling results for the 1964-type Alaska tsunami gave the following main results: (1) The tsunami at the Victoria Coast Guard Facility will reach **0.56 m** above the tidal level or (0.56 m + 0.73 m) = **1.29 m** above mean sea level at the time of the wave arrivals, with the first wave being the highest wave; (2) The distribution of tsunami wave amplitudes in Victoria Harbour and the vicinity of the Victoria Coast Guard Facility will be nearly spatially uniform [*Fine et al.*, 2018a].

For the 1700-type CSZ tsunami, *Fine et al.* [2018b] used two models of the earthquake rupture type and tsunami source region: Model A is a buried rupture and Model B a splay-faulting rupture. Model B generates higher waves in the Victoria area than Model A. Therefore, Model B can be considered as the "worst case scenario" for the region.

The main findings of *Fine et al.* [2018b] are the following: (1) The maximum wave amplitudes at the Coast Guard Base will be **1.72 m** (Model A) and **2.26 m** (Model B) above the tidal level at the time of the event, or (0.2+1.72+0.73) m = **2.65 m** for Model A and (0.2+2.26+0.73) m = **3.19 m** for Model B above the mean sea level at the time of the event (0.2 m is the land subsidence expected to

occur at the time of the CSZ earthquake); (2) the first-crest wave will be the highest wave; the maximum tsunami wave heights will occur from 1h 25 min to 1 h 30 min after the earthquake; (3) tsunami wave periods will range from 25 to 70 min; (4) tsunami wave amplitudes will be nearly spatially uniform throughout Victoria Harbour and at the Coast Guard Base location; and (5) sea level will drop ~0.2 m immediately after the start of the earthquake due to land subsidence and the leading tsunami wave trough will cause the water level to temporarily fall an additional 1 m below tidal level as it passes.

Because many of the details of future possible tsunamis remain unknown, including the tidal level at the time of the event, seasonal variations, uncertainties in the earthquake source distribution, possible storm surge or other oceanic events, *Fine et al.* [2018a,b] recommend that a safety factor of 50% be added giving an estimated tsunami-generated sea level height of **1.94 m** =1.5×(0.56 m+0.73 m) for a 1964-type Alaska tsunami and **4.79 m** =1.5×(2.26 m+0.73 m +0.2 m) for a Model B-type CSZ tsunami (the worst-case scenario).

Global sea level rise is an important additional factor influencing the tsunami risk for the British Columbia coast, including Victoria Harbour. Recently, the United Nations' Intergovernmental Panel on Climate Change (IPCC) published several reports and adopted Representative Concentration Pathway (RCP) scenarios for greenhouse gas concentration trajectories: **RCP2.6**, **RCP4.5**, **RCP6**, and **RCP8.5**. Based on these scenarios, *James et al.* [2015; 2021] and *Lemmen et al.* [2016] prepared special reports considering sea level rise in western Canada, focussing on the coast of British Columbia, which take into account both global climatic sea level rise and vertical tectonic motions. *Rabinovich and Thomson* [2020] used these results to evaluate expected sea level changes along the southeastern coast of Vancouver Island for *low*, *moderate* and *high* global sea level rise scenarios. All these findings allowed us to estimate the general spatial structure of projected relative sea-level changes in Juan de Fuca Strait and, specifically, in the Victoria region.

The following RCP-dependent apply to sea level rises at the Victoria Coast Guard Station:

- *Low* (RCP2.6): 0.15 m (2050), 0.36 m (2100) and 1.10 m (2200);
- *Moderate* (RCP4.5): 0.155 m (2050), 0.40 m (2100) and 1.25 m (2200);
- *High* (RCP8.5): 0.16 m (2050), 0.55 m (2100) and 1.75 m (2200).

Lastly , we combine the results of the numerical modelling of the 1964-type Alaska tsunami and the 1700-type CSZ tsunami with the expected sea level changes in Victoria for 2100 to obtain the following tsunami wave heights relative to the tide at the time of the event:

	Alaska	CSZ
Low (RCP2.6)	(1.29 m + 0.36 m) = **1.65 m**	(3.19 m + 0.36 m) = **3.55 m**
Moderate (RCP4.5)	(1.29 m + 0.40 m) = **1.69 m**	(3.19 m + 0.40 m) = **3.59 m**
High (RCP8.5)	(1.29 m + 0.55 m) = **1.84m**	(3.19 m + 0.55 m) = **3.74 m**

Because many of the details of future possible tsunamis remain unknown, both in local background oscillations and the earthquake source parameters, *Fine et al.* [2018a,b] recommend addition of a safety factor of 50% to the estimated tsunami-generated sea level heights. The total effective wave heights in that case will be:

	Alaska	CSZ
Total (RCP2.6)	**2.30 m**	**5.15 m**
Total (RCP4.5)	**2.34 m**	**5.19 m**
Total (RCP8.5)	**2.49 m**	**5.34 m**

All these predictions are for 2100; for 2200 we need to add ~**0.85 m** for RCP4.5 and **1.2 m** for RCP8.5.

Finally, *James et al*. [2021] specify an *enhanced RCP8.5 scenario* the projected sea level at 2100 that provides an additional **65 cm** of global sea-level rise relative to the median projection of RCP8.5 sourced from possible melting of the West Antarctic Ice Sheet.

REFERENCES

AECOM (2013), *Modelling of Potential Tsunami Inundation Limits and Run-Up*, Capital Regional District, Project No. 6024 2933, 36 p.

Atwater, B.F., Musumi-Rokkaku, S., Satake, K., Tsuji, Y., Ueda, K., and Yamaguchi, D.K., (2005), *The Orphan Tsunami of 1700—Japanese Clues to a Parent Earthquake in North America*, U.S. Geological Survey Professional Paper No. 1707, 133 p.

Bornhold, B.D. and Thomson, R.E. (2013), Trends in sea level; In *Climate Trends and Projections for the Pacific Large Aquatic Basin*, (ed.) J.R. Christian and M.G.G. Foreman; Can. Tech. Rep. Fish. Aquatic Sci. 3032, 113 p.

Bush, E. and Lemmen, D.S., editors (2019), *Canada's Changing Climate Report*; Government of Canada, Ottawa, ON. 444 p. Available online at: https://changingclimate.ca/CCCR2019/.

Church, J.A., Clark, P.U. Cazenave, A. et al. (2013a). Sea Level Change. In: *Climate Change 2013: The Physical Science Basis*. Contribution of Working Group I to the Fifth Assessment Report of the Intergovernmental Panel on Climate Change [T.F. Stocker et. al eds.]. Cambridge University Press, Cambridge, United Kingdom and New York, NY, USA.

Church, J.A., Clark, P.U. Cazenave, A. et al. (2013b), Sea Level Change: Supplementary Materials. In: *Climate Change 2013: The Physical Science Basis*. Contribution of Working Group I to the Fifth Assessment Report of the Intergovernmental Panel on Climate Change [T.F. Stocker et. al eds.]. Cambridge University Press, Cambridge, United Kingdom and New York, NY, USA.

Cherniawsky, J.Y., Titov, V.V., Wang, K., and Li, J.-Y. (2007), Numerical simulations of tsunami waves and currents for southern Vancouver Island from a Cascadia megathrust earthquake, *Pure and Applied Geophysics*, 164 (2-3), 465-492, doi:10.1007/s00024-006-0169-0.

Cheung, K.F., Wei, Y., Yamazaki, Y., and Yim, S.C.S. (2011), Modeling of 500-year tsunamis for probabilistic design of coastal infrastructure in the Pacific Northwest, *Coastal Engineering*, 58, 970–985.

Clague, J.J., Bobrowsky, P.T., and Hutchinson, I. (2000), A review of geological records of large tsunamis at Vancouver Island, British Columbia, and implications for hazard, *Quaternary Science Reviews*, 19, 849-863.

Clague, J.J., Munro, A., and Murty, T.S. (2003), Tsunami hazard and risk in Canada, *Natural Hazards*, 28(2-3), 407-434.

Dunbar, D., LeBlond, P., and Murty, T.S. (1991), Evaluation of tsunami amplitudes for the Pacific coast of Canada. *Progress in Oceanography*, 26, 115-177.

Fine, I.V., Cherniawsky, J.Y., Rabinovich, A.B., and Stephenson, F.E. (2008), Numerical modeling and observations of tsunami waves in Alberni Inlet and Barkley Sound, British Columbia, *Pure and Applied Geophysics*, 165(11/12), 2019-2044.

Fine, I.V., Kulikov, E.A., and Cherniawsky, J.Y. (2013), Japan's 2011 tsunami: Characteristics of wave propagation from observations and numerical modelling. *Pure and Applied Geophysics*, 170, 1295-1307.

Fine, I.V., Cherniawsky, J.Y., Thomson, R.E., Rabinovich, A.B., and Krassovski, M.V. (2015), Observations and numerical modeling of the 2012 Haida Gwaii tsunami off the coast of British Columbia, *Pure and Applied Geophysics*, 172(3-4), 699-718; doi: 10.1007/s00024-014-1012-7.

Fine, I.V., Thomson, R.E., Lupton, L.M., and Mundschutz, S. (2018a), *Numerical Modelling of an Alaska 1964-type Tsunami at the Canadian Coast Guard Base in Victoria, British Columbia*, Can. Tech. Rep. Hydr. Ocean Sci. 323, Fisheries and Oceans Canada, Institute of Ocean Sciences, Sidney, BC.

Fine, I.V., Thomson, R.E., Lupton, L.M., and Mundschutz, S. (2018b), *Numerical Modelling of a Cascadia Subduction Zone Tsunami at the Canadian Coast Guard Base in Victoria, British Columbia*, Can. Tech. Rep. Hydr. Ocean Sci.324, Fisheries and Oceans Canada, Institute of Ocean Sciences, Sidney, BC.

Gao, D. (2016), *Defining Megathrust Tsunami Sources at Northernmost Cascadia Using Thermal and Structural Information*. Master of Science Thesis, School of Earth and Ocean Sciences, The University of Victoria; https://dspace.library.uvic.ca/handle/1828/7435

Hausfather, Z. and Peters, G.P. (2020), Emissions – the 'business as usual' story is misleading, *Nature*, 577, 618-620.

Imamura, F. (1996), Review of tsunami simulation with a finite difference method. In: *Long-Wave Run-up Models* (Eds. H. Yeh, P. Liu, and C. Synolakis), World Scientific, Singapore, pp. 25–42.

Imamura, F., Yalciner, A.C., and Ozyurt, G. (2006), *Tsunami Modelling Manual (TUNAMI Model)*; http://www.tsunami.civil.tohoku.ac.jp/hokusai3/J/projects/manual-ver-3.1.pdf

James, T.S., Henton, J.A., Leonard, L.J., Darlington, A., Forbes, D.L., and Craymer, M. (2014), *Relative Sea-level Projections in Canada and the Adjacent Mainland United States*; Geological Survey of Canada, Open File 7737, 72 p. doi:10.4095/295574.

James, T.S., Henton, J.A., Leonard, L.J., Darlington, A., Forbes, D.L., and Craymer, M. (2015), *Tabulated values of Relative Sea-Level Projections in Canada and the Adjacent Mainland United States*; Geological Survey of Canada, Open File 7942, 81 p. doi:10.4095/297048.

James, T.S., Robin, C., Henton, J.A., and Craymer, M. (2021), *Relative Sea-Level Projections for Canada Based on the IPCC Fifth Assessment Report and the NAD83v70VG National Crustal Velocity Model*; Geological Survey of Canada, Open File 8764, 1 .zip file, https://doi.org/10.4095/327878.

Johnson, J.M., Satake, K., Holdahl, S.R., and Sauber, J. (1996), The 1964 Prince William Sound earthquake – joint inversion of tsunami waveforms and geodetic data, *Journal of Geophysical Research*, 101 (B1), 523-532.

Lander, J.F. (1996), *Tsunamis Affecting Alaska*, 1737-1996. USDC/NOAA, Boulder, CO, USA, 195 p.

LeBlond, P.H., Dunbar, D., and Murty, T.S. (1989), Maximum tsunami amplitudes and associated currents on the coast of British Columbia, *Science of Tsunami Hazards*, 7(1). 3-44.

Lemmen, D.S., Warren, F.J., James, T.S., and Mercer Clarke, C.S.L., editors (2016). *Canada's Marine Coasts in a Changing Climate*; Government of Canada, Ottawa, ON, 274p.

Leonard, L.J., Rogers, G.C., and Mazzotti, S., (2014), Tsunami hazard assessment of Canada, *Natural Hazards*, 70, 237-274.

Liu, P.L.-F., Woo, S-B. and Cho, Y.-S. (1998). *Computer Programs for Tsunami Propagation and Inundation.* Technical report, Cornell University.

Meinshausen, M. et al. (2011), The RCP greenhouse gas concentrations and their extensions from 1765 to 2300 (open access), *Climatic Change*, 109(1–2), 213–241; doi:10.1007/s10584-011-0156-z

Moss, R. et al. (2008). Towards New Scenarios for Analysis of Emissions, Climate Change, Impacts, and Response Strategies (PDF). Geneva: Intergovernmental Panel on Climate Change. p. 132.

Myers, E.P. and Baptista, A.M. (2001), Analysis of factors influencing simulations of the 1993 Hokkaido Nansei-Oki and 1964 Alaska Tsunamis. *Natural Hazards*, 23, 1-28; https://doi.org/10.1023/A:1008150210289

Ng, M.K.-F., LeBlond, P.H., and Murty, T.S. (1991), Simulation of tsunamis from great earthquakes on the Cascadia subduction zone, *Science*, 250, 1248–1251.

Oppenheimer, M. and Glavovic, B. (Lead authors) (2019), Sea Level Rise and Implications for Low Lying Islands, Coasts and Communities. Chapter 4. In: *IPCC Special Report on the Ocean and Cryosphere in a Changing Climate (SROCC)*, https://www.ipcc.ch/reports/

Rabinovich, A.B. and Stephenson, F.E. (2004), Longwave measurements for the coast of British Columbia and improvements to the tsunami warning capability, *Natural Hazards*, 32(3), 313-343.

Rabinovich, A.B., Thomson, R.E., Krassovski, M.V., Stephenson, F.E., and Sinnott, D.C. (2019), Five great tsunamis of the 20th century as recorded on the coast of British Columbia, *Pure and Applied Geophysics*, 176(7), 2887-2924; doi: 10.1007/s00024-019-02133-3.

Rabinovich, A.B. and Thomson, R.E. (2020), *Effect of Global Sea Level Rise over the near, Intermediate and Long-Term on Extreme Longwave Motions on IOS (Patricia Bay) and PBS (Nanaimo)*, Unpublished report, Fisheries and Oceans Canada, Institute of Ocean Sciences, Sidney, BC.

Robin, C.M.I., Craymer, M., Ferland, R., James, T.S., Lapelle, E., Piraszewski, M., and Zhao, Y. (2020), *NAD83v70VG: A New National Crustal Velocity Model for Canada*; Geomatics Canada, Open File 0062, 1. zip file. https://doi.org/10.4095/327592

Rogelj, J., Meinshausen, M., and Knutti, R. (2012), Global warming under old and new scenarios using IPCC climate sensitivity range estimates, *Nature Climate Change*, Vol.2, p. 248–253; doi:10.1038/NCLIMATE1385.

Satake, K., Shimazaki, K., Tsuji, K., and Ueda, K. (1996), Time and size of a giant earthquake in Cascadia earthquake inferred from Japanese tsunami records of January 1700, *Nature*, 379, 246–249.

Stephenson F.E. and Rabinovich, A.B. (2009), Tsunamis on the Pacific coast of Canada recorded in 1994-2007, *Pure and Applied Geophysics*, 166(1/2), 177-210.

Suito, H. and Freymueller, J.T. (2009). A viscoelastic and afterslip post seismic model for the 1964 Alaska earthquake. *Journal of Geophysical Research*, 114, B11404, doi:10.1029/2008JB005954.

Suleimani, E.N. (2011). *Numerical Studies of Tectonic and Landslide-Generated Tsunamis Caused by the 1964 Great Alaska Earthquake*, University of Alaska Fairbanks, Ph.D. thesis, 181 p.

Suleimani, E.N., Nicolsky, D.J., and Koehler, R.D. (2013), *Tsunami Inundation Maps of Sitka, Alaska*, Report of Investigations 2013-3, State of Alaska, Department of Natural Resources, Division of Geological and Geophysical Surveys, Fairbanks, AK, 76 p. doi:10.14509/26671.

Thomson, R.E. (1981), *Oceanography of the British Columbia Coast*. Can. Special Pub. Fish. Aquat. Sci., 56. Ottawa, 291 p.

Thomson, R.E., Bornhold, B.D., and Mazzotti, S. (2008), *An Examination of the Factors Affecting Relative and Absolute Sea Level in Coastal British Columbia*; Can. Tech. Rep. Hydr. Ocean Sci. 260, 49 p.; http://www.dfo-mpo.gc.ca/Library/335209.pdf

Thomson R.E. and Emery, W.J. (2014), *Data Analysis Methods in Physical Oceanology*, Third Edition, Elsevier, New York, 716 p.

Vadeboncoeur, N. (2016), Perspectives on Canada's West Coast region; in Canada's Marine Coasts in a *Changing Climate*, (ed.) D.S. Lemmen, F.J. Warren, T.S. James and C.S.L. Mercer Clarke; Government of Canada, Ottawa, ON, pp. 207-252.

Wang, K., Wells, R., Mazzotti, S., Hyndman, R.D., and Sagiya T., (2003), A revised dislocation model of interseismic deformation of the Cascadia subduction zone, *Journal of Geophysical Research*, 108(B1), doi:10.1029/2001JB001227.

Wang, K., and Tréhu, A.M. (2016), Invited review paper: Some outstanding issues in the study of great megathrust earthquakes—The Cascadia example, *Journal of Geodynamics*, 98, 1-18.

Wang, P-L., Engelhart, S.E., Wang, K., Hawkes, A.D., Horton, B.P., Nelson, A.R., and Witter, R.C. (2013), Heterogeneous rupture in the Great Cascadia earthquake of 1700 inferred from coastal subsidence estimates. *Journal of Geophysical Research*, 118, 2460-2473.

Weart, S. (2011), *International Cooperation: Democracy and Policy Advice* (1980s). The Discovery of Global Warming. American Institute of Physics.

Weyant, J., Azar, C., Kainuma, M. et al. (2009), Report of 2.6 Versus 2.9 Watts/m2. RCPP Evaluation Panel (PDF). Geneva, Switzerland: IPCC Secretariat.

Whitmore, P.M. (1993), Expected tsunami amplitudes and currents along the North American coast for Cascadia Subduction Zone earthquakes, *Natural Hazards*, 8, 59–73.

Wigen, S.O. (1983), Historical studies of tsunamis at Tofino, Canada, in Tsunamis – Their Science and Engineering, edited by K. Iida and T. Iwasaki, Terra Sci. Publ. Comp., Tokyo, Japan, 105-119.

Wigen, S.O. and White, W.R.H. (1964), *Tsunami of March 27-29, 1964, West Coast of Canada*, Dept. Mines Techn. Surv., Victoria, BC, Canada, 12 p.

Witter, R.C., Zhang, Y.J., Wang, K. et al. (2013), Simulated tsunami inundation for a range of Cascadia megathrust earthquake scenarios at Bandon, Oregon, USA, *Geosphere*, 9 (6), 1783-1803; doi:10.1130/GES00899.1